Ore Geology Reviews 91 (2017) 153–172

Contents lists available at ScienceDirect

Ore Geology Reviews

journal homepage: www.elsevier.com/locate/oregeorev

Geochemistry, fluid inclusion and stable isotope constraints (C and O) of the Sivrikaya Fe-skarn mineralization (Rize, NE Turkey)

Yılmaz Demir[a,*], İbrahim Uysal[b], Raif Kandemir[a], Andrea Jauss[c]

[a] Recep Tayyip Erdogan University, Department of Geological Engineering, 53100 Rize, Turkey
[b] KTÜ Department of Geological Engineering, 61100 Trabzon, Turkey
[c] WITec GmbH, Lise Meitner Strasse 6, 89081 Ulm, Germany

ARTICLE INFO

Keywords:
Sivrikaya Fe–skarn
Fluid inclusion
C and O isotopes
Rize
NE Turkey

ABSTRACT

The Sivrikaya Fe-skarn mineralization is hosted by dolomitic limestone layers of Late Cretaceous volcano-sedimentary unit, comprised of andesite, basalt and their pyroclastites, including, sandstone, shale and dolomitic limestone layers. Intrusion of the Late Cretaceous–Eocene İkizdere Granitoid in the volcano–sedimentary unit resulted in skarn mineralization along the granitoid–dolomitic limestone contact. The ore is associated with exoskarns, and mineralization is characterized by early anhydrous garnet and pyroxene with late hydrous minerals, such as epidote, tremolite, actinolite and chlorite. The ore minerals are mainly magnetite and hematite, with minor amounts of pyrite and chalcopyrite. The composition of garnet and pyroxene in the exoskarn is $Adr_{79.45-99.03}Grs_{0-17.9}Prs_{0.97-2.65}$ and $Di_{69.1-77.1}Hd_{22.2-29.8}Jhn_{0.6-1.4}$, respectively, and abundances of magnetite in the ore suggest that the Fe-skarn mineralization formed under relatively oxidized conditions.

Homogenization temperatures (T_h) of all fluid inclusions and calculated salinity content are in the range of 166 °C–462 °C and 0.35–14.3 wt% NaCl equ., respectively. Well-defined positive correlation between Th and salinity values indicates that meteoric water was involved in the hydrothermal solutions. Eutectic temperatures (Te) between −40.8 °C and −53.6 °C correspond to the presence of $CaCl_2$ in the early stage of fluid inclusions. On the other hand, the Te temperatures of later-stage fluid inclusions, in the range of −38 °C and −21.2 °C, correspond to the presence of $MgCl_2$, $FeCl_2$, KCl and NaCl type salt combinations. None of the fluid inclusions were found to contain separated gas phases in microscopy observations. However, a limited amount of dissolved CH_4 was identified in the early stage, high temperature fluid inclusions using Raman spectroscopic studies.

$\Delta^{18}O$ values in both dolomitic limestone (10.8–12.5‰) and skarn calcite (7.6–9.8‰) were highly depleted compared to the typical $\delta^{18}O$ values of marine limestones. Decreases in $\delta^{18}O$ values are accepted as an indication of dilution by meteoric water because retrograde brecciation of garnet, magnetite and breccia filling epidote and quartz in volcanic host rocks are an indication of increasing permeability, allowing infiltration of meteoric water. Highly depleted $\delta^{13}C$ isotopes (up to −6.5‰) of dolomitic limestone, indicate that organic matter in carbonates had an effect on the decreasing isotopic ratios. The presence of CH_4 and CH_2 in fluid inclusions can be explained by the thermal degradation of these organic materials.

1. Introduction

The Northeastern Metallogenic Belt is one of the most important mining regions in Turkey, including volcanogenic massive sulfide, hydrothermal vein, skarn and porphyry-type ore deposits. Most academic studies and mining activities have primarily focused on massive sulfide (Özgür, 1993; Akçay and Arar, 1999; Tüysüz, 2000; Gökce, 2001; Gökçe and Spiro, 2000, 2002; Çiftçi and Hagni, 2005; Revan, 2010; Demir et al., 2013; Sağlam and Akçay, 2016) and hydrothermal-type deposits (Tüysüz et al., 1995; Akçay and Çavga, 1997; Demir et al., 2008; Aslan and Akçay, 2011; Yaylali-Abanuz et al., 2012; Demir et al., 2015), due to their higher economic importance.

On the other hand, the geological properties of this region are especially fertile for the formation of skarn-type deposits due to the large area of Early Cretaceous limestones (Berdiga Formation) and limestone layers in Late Cretaceous volcano-sedimentary unit at the contact with younger granitic intrusions over a long distance. Metasomatic processes between these granitic intrusions and limestones have resulted in skarn-type deposits in the region. Some of these commonly known skarn locations are Çambaşı (Ordu), Kotana,

* Corresponding author.
E-mail address: yilmaz.demir@erdogan.edu.tr (Y. Demir).

http://dx.doi.org/10.1016/j.oregeorev.2017.10.008
Received 30 March 2017; Received in revised form 6 October 2017; Accepted 10 October 2017
Available online 14 October 2017

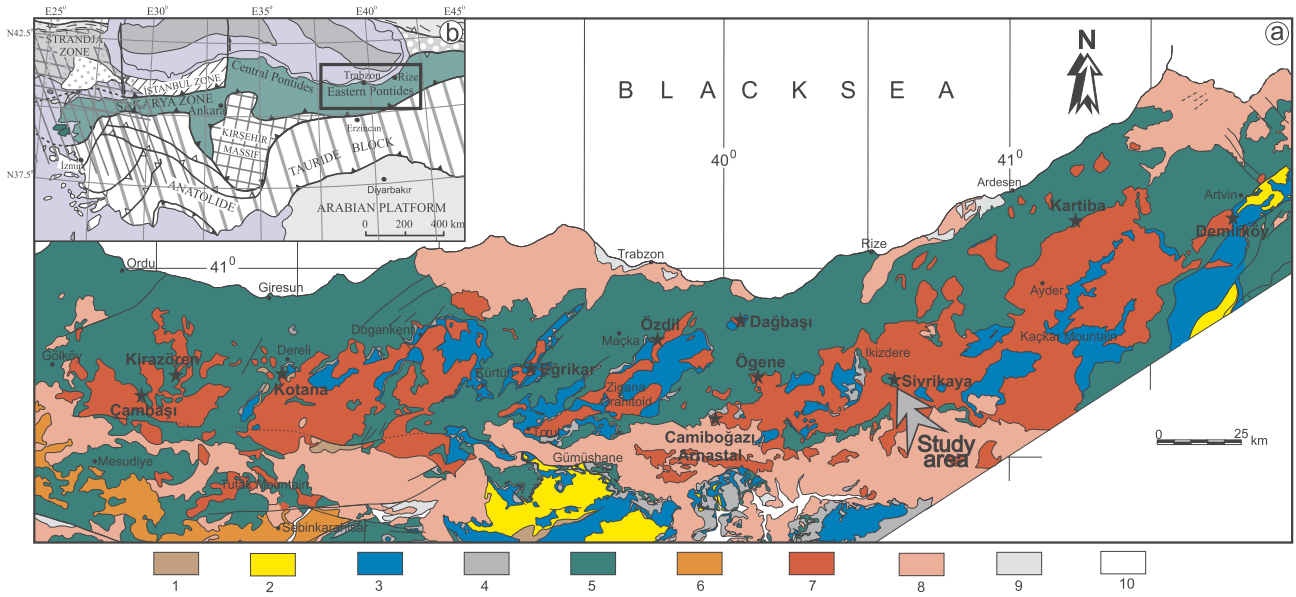

Fig. 1. Major contact metasomatic occurrences and associated lithological units along the northeastern region of Turkey (modified from Güven, 1993).

Kirazören (Giresun), Ögene, Özdil, Dağbaşı (Trabzon), Kartiba, Sivrikaya (Rize), Demirköy (Artvin), Eğrikar, Camiboğazı and Arnastal (Gümüşhane) (Fig. 1a).

These skarn mineral systems have been investigated in earlier studies (Aslan, 1991; Hasançebi, 1993; Saraç, 2003; Çiftçi, 2011; Sipahi, 2011; Kurt, 2014), and some important differences were reported in terms of geology, mineralogy, skarnization processes and ore–host rock interactions. Exoskarn-type mineralizations were reported from Özdil (Trabzon), Kartiba (Rize), Çambaşı (Ordu), Kotana (Giresun), Arnastal and Camiboğazı (Gümüşhane) locations, whereas both exoskarn- and endoskarn-type mineralizations were reported from Kirazören (Giresun) and Ögene (Trabzon) locations. In terms of ore mineralogy, oxide minerals (magnetite and hematite) constitute the main ore mineral assemblages in the locations of Özdil, Kartiba and Camiboğazı. However, both oxide and sulfide mineral assemblages were reported from the Arnastal, Kotana, Kirazören and Dağbaşı areas. In addition to these examined skarn mineralizations, some less investigated skarn-type occurrences also exist in the region. Nevertheless, little effort has been made to understand the mineralogical and geochemical properties of skarn mineral systems compared to other types of deposits.

Although the Sivrikaya deposit is one of the better-known skarns (Çakır, 1986; Çınar et al., 1986) in the region, there has been no detailed mineralogical, petrographical and geochemical investigation of this mineralization. In addition to geological and mineralogical properties, the present paper deals with the composition of skarn minerals, microthermometric characteristics of fluid inclusions, and oxygen and carbon isotope composition of skarn carbonates and calcites. Thus, the physico–chemical condition of the Sivrikaya skarn deposit is investigated. This research will provide greater information on the geological settings and future prospects for this type of deposit at a regional scale.

2. Geological settings

Turkey is one of the major region of the Alpine–Himalayan orogenic system. North of the İzmir–Ankara–Erzincan suture in Turkey are three tectonic units, the Strandja Masif, the İstanbul Zone and the Sakarya Zone, which were assembled at three different times (Okay and Şahintürk, 1997). The eastern part of the Sakarya Zone is called the Eastern Pontides (Fig. 1b), a geographic name describing the eastern section of the Pontide mountain chain, which also corresponds to the eastern Sakarya Zone.

The northeastern region of the Sakarya Zone consists of metamorphic, plutonic, sedimentary, volcanic and volcano-sedimentary rocks ranging in age from Paleozoic to Cenozoic. High temperature/low pressure quartz–feldspathic gneiss and schist as well as low- to medium-temperature amphibolite, phyllite, chert, marble and minor metaperidotite with Early Carboniferous metamorphic ages are the oldest units in the Hercynian basement (Topuz et al., 2007; Dokuz, 2011; Dokuz et al., 2015). Numerous small granitoids ofmiddle Carboniferous to Early Permian ages are emplaced in these metamorphic rocks throughout the Sakarya Zone (Dokuz et al., 2017; Topuz et al., 2010). Both metamorphic and granitic rocks crop out in the southern part of the Sakarya Zone.

The Early to Middle Jurassic Şenköy Formation (Kandemir, 2004) is deposited unconformably over the heterogeneous Hercynian basement. This formation consists of andesite, basalt, lithic tuff, volcanogenic sandstone, shale, conglomerate and Ammonitico Rosso-type sediments and limestone (Kandemir and Yılmaz, 2009). The Şenköy Formation is overlain conformably by a Late Jurassic–Early Cretaceous Berdiga Formation, which was largely characterized by platform-type carbonates (Pelin, 1977; Yılmaz and Kandemir, 2006). After the deposition of the Early–Middle Jurassic Şenköy Formation under tectonically active conditions, these platform-type carbonates accumulated into the rift basin as a result of a decrease in tectonic activity (Yılmaz and Kandemir, 2006). The Berdiga Formation consists of medium- to massive-bedded grey to yellowish limestones. The lower and middle parts of the formation are made up of oncolitic, intraclastic packstones and grainstones, while the upper part is characterized by packstones and grainstones containing abundant small benthic foraminiferas, fragments of molluscs and echinoids (Vörös and Kandemir, 2011). The structural and sedimentological properties of the Berdiga Formation suggest that the sediments of this unit were probably deposited within a shallow carbonate shelf environment during the Late Jurassic–Early Cretaceous period (Yılmaz et al., 2008).

The Late Mesozoic lithostratigraphy is dominated by widespread plutonic, subvolcanic and volcano-sedimentary rocks, which host numerous volcanogenic massive sulfide deposits at the northern Sakarya

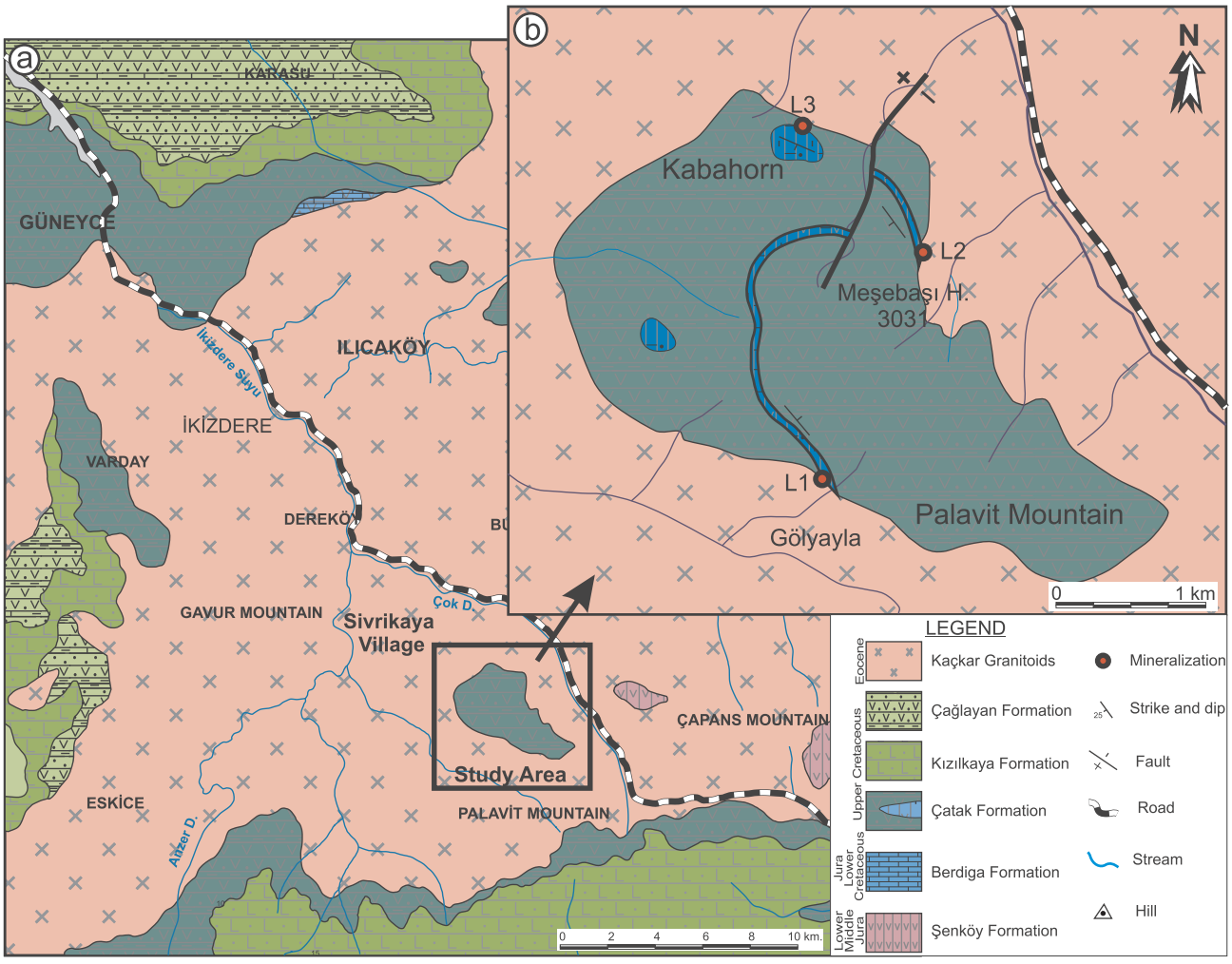

Fig. 2. Geological map (modified from Güven, 1993) and ore locations around the İkizdere (Rize) region.

Zone (Karslı et al., 2010a,b). The volcano-sedimentary sequence comprises five units, Çatak, Kızılkaya, Çağlayan, Tirebolu (Güven, 1993) and Tonya formations (Korkmaz, 1993). The Çatak Formation is composed of andesite, basalt and tuffs intercalated with clayey, sandy and Globotruncana-bearing pelagic limestones. According to Sofracıoğlu and Kandemir (2013), this formation contains large limestone boulders of Late Jurassic–Early Cretaceous Berdiga Formation. The Kızılkaya Formation similarly shows volcano-sedimentary features. However, it is characteristically separated from the Çatak Formation by its dacitic and rhyodacitic nature and minor clayey and sandy limestone intercalations. The Çağlayan Formation conformably overlies the Kızılkaya Formation and consists of marls, sandstones and sandy limestones alternating with spilitic basalts, andesite and their pyroclastites (Kırmacı and Akdağ, 2005). The Kızılkaya Formation conformably overlies the Tirebolu Formation, which consists of rhyodacite and its pyroclastics, including red pelagic micritic limestone layers. The Tonya Formation is the uppermost Mesozoic sequence and contains shelf derived carbonate clast, intrabasinal lithoclasts with extrabasinal pebbles and basaltic and andesitic volcanic boulders (Sofracıoğlu and Kandemir, 2013). The Eocene-aged Kabaköy Formation unconformably overlies these Late Cretaceous volcano-sedimentary units and consists of andesite, basalt and their associated pyroclastics, with lesser amounts of sandstones, sandy limestones and tuffite (Aydin, 2014).

Moreover, many different younger granitoid intrusions which are part of the composite Kaçkar Batholith have been described from northeastern Turkey. The age of these intrusions ranges from Late Jurassic (Şengör et al., 1980; Dokuz et al., 2010) through Late Cretaceous (Kaygusuz et al., 2009; Karslı et al., 2004; Topuz et al., 2007; Okay and Şahintürk, 1997; Karslı et al., 2011) to Early Eocene (Karslı et al., 2010b; Karslı et al., 2007; Moore et al., 1980; Boztuğ et al., 2004). Recent studies (Boztuğ et al., 2006; Karslı et al., 2004, 2010a; Kaygusuz et al., 2009) have shown that the composition of these intrusions varies from low-K tholeitic to high-K calc–alkaline and peraluminous to alkali monzonite and syenites.

2.1. Ore geology of the Sivrikaya skarn deposit

The Sivrikaya area is located in the northern part of the Black Sea Region and contains extensive Mesozoic and Cenozoic units. Volcano-sedimentary rocks of the Liassic Şenköy Formation form the basement in the area, and these are conformably overlain by neritic limestones of the Late Jurassic–Early Cretaceous Berdiga Formation. Regular alternation of mafic and felsic volcano-sedimentary rocks deposited during the Late Cretaceous in the region is a result of active volcanism (Güven, 1993, 1998). The mafic volcano-sedimentary unit at the bottom level of this alternation corresponds to the Çatak Formation and conformably overlies the Berdiga Formations.

The Çatak Formation consists of andesite, basalt and their pyroclastites. Dark grey volcanics are generally fractured and contain vesicles. The volcanics are also generally altered, and epidote, chlorite, sericite and calcites are common alteration products. These volcanics include an interlayered sedimentary sequence. This sequence starts with light grey sandy limestone, dolomitic limestone, grades upward thin layers of reddish limestone, sandstone, claystone, marl and

limestone alternation, with interbedded tuffite. The age of these rocks has been accepted as Turonian–Santonian based on the paleontological evidence of *Globotruncana lapparenti, Globotruncana linneiana, Globotruncana* sp., *Marginotruncana* sp., *Globigerinella* sp., *Globigerinelloides* sp., *Gumbelina* sp. and *Hedbergella* sp. observed in reddish limestone levels (Güven, 1998). Moving upwards, a felsic volcano-sedimentary level corresponds to the Kızılkaya Formation, and repeated mafic volcano-sedimentary levels at the upper side also correspond to the Çağlayan Formation. These Kızılkaya and Çağlayan formations were observed in the surrounding area, and they have no relation to the skarnizations.

The emplacements of the İkizdere Pluton, which is a part of composite Kaçkar Batholith, caused the skarnization along the limestone layers of the volcano-sedimentary units and the granite pluton contact areas (Fig. 2). The pluton was dated at 76.21 ± 0.79 million years using the U/Pb SHRIMP method by Evcimen (2011). The İkizdere Pluton is made of granite, granodiorite, tonalite, quartz monzonite and diorite, with granodiorite and tonalite dominance at ~70% of the total volume. Monzonite and diorite occupy less than 25% of the total volume, and granite never exceeds 10%. All the rock types have similar mineral paragenesis, and these minerals consist of plagioclase, quartz, K-feldspar, amphibole, biotite, pyroxene (mostly clinopyroxene) and Fe–Ti oxides, in descending order of abundance.

Three different skarn mineralizations (L1: Gölyayla, L2: Meşebaşı Hill and L3: Kabahorn; Fig. 2a and b) are located along the boundary between carbonate rock layers (in the lower mafic volcano-sedimentary Çatak Formation) and İkizdere granodiorite intrusion. The skarn mineralization can be observed along the carbonate layer, which extends up to one hundred meters horizontally and is a few meters thick. Banded ore is the most common ore texture along the carbonate layers (Fig. 3a). Discontinuous ore pockets reaching up to 10 meters are also present (Fig. 3b). Massive ore texture is common in these ore pockets. These carbonate-controlled features of the skarn at each location belong to exoskarn-type mineralization.

The skarn zone is commonly fractured. Ore fragments with sedimentary blocks including limestone, sandstone, marl and tuff are distributed along the mountain slope. Andesitic and basaltic volcanic rocks beneath the sedimentary units were brecciated close to the ore body. Quartz and alteration product epidote are commonly observed in these andesite and basalt breccias (Fig. 3c). In addition to brecciation, intensive fracturing is also observable in this zone. Fracture-filling-type magnetite occurrences along this zone represent subsequent grade skarn development (Fig. 3d). Dolomitic limestones along the skarn zone contain organic material both at the macroscopic (Fig. 3e) and microscopic scales (Fig. 3f). No decisive descriptions of the initial forms of these fossil species were possible due to excessive carbonatization.

2.2. Mineralogical and textural properties

The Sivrikaya skarn includes a variety of macroscopic-scale prograde patterns. Sporadically nodular magnetite and hematite assemblages a few centimeters in scale are accompanied by garnet (Fig. 3g), quartz and epidote (Fig. 3h) at the marble–skarn contact. Magnetite branches in the light-colored marble are observable along the skarn carbonates, indicating mossy textures (Fig. 3i). Rhythmic intergrowth of magnetite and epidote was observed in the marble–skarn contact, which is centimeters to decimeters thick (Fig. 3j). The other macroscopic prograde textures are characterized by nodule-shaped morphologies at the marble–skarn contact. The first type of reactive infiltration nodule is characterized by irregular garnet aggregates in skarn carbonates (Fig. 3k). This type of garnet aggregate is observed close to the ore body, ranging from centimeters to decimeters in scale. Second-type nodule is described as silica infiltration chert in skarn carbonates reaching up to 0.5 meters in scale. The outer shell of these chert nodules is always surrounded by a calcite layer of a few centimeters (Fig. 3l). This type of chert nodule is also accepted as an indication of prograde ore textures (Joesten, 1974; Ciobanu and Cook, 2004).

Skarn zones are dominated by garnet, with a limited amount of clinopyroxenes. Two types of garnets were distinguished in petrographical studies. The first type consists of euhedral to subhedral coarse-grained crystals with brown and reddish-brown colors. This type of garnet is always included in iron-free carbonates (Figs. 3k and 4a). The second type of garnet is observed in subhedral to anhedral fine-grained forms and always accompanied by iron ore. This type of garnet is either cut by hematite (Fig. 4b) or found in the form of inclusions in later-stage magnetite (Fig. 4c). Oscillatory zoning was microscopically identified in these types of garnets as a prograde texture in the marble–skarn contact (Fig. 4b and d). Another prograde texture at the microscopic scale is magnetite coarsening towards boundaries with garnets (Fig. 4c). In this type of texture, highly populated small-sized garnet clusters were coupled in coarse magnetite grains in unstable conditions of reaction fronts along the skarn border (Joesten, 1991; Ortoleva, 1994).

Ore in the Sivrikaya area consists of hematite and magnetite, and these minerals mainly coexist with garnet, quartz and epidote. Hematite is observable in needle shaped, lamellar, oriented and radial forms. Replacement of these radial hematites by carbonates was commonly observed in magnetite-free samples. Magnetite is observable mostly in euhedral, granular and (to a lesser extent) elongated crystal forms. These magnetites cut needle-shaped, oriented hematites (Fig. 4e). Limited amounts of pyrite and chalcopyrite grains are also included in these magnetites (Fig. 4e and f).

Replacement–overgrowth relationships were observed at the border of hematite with magnetites (Fig. 4f–h). This texture indicates at least two cycles of stability inversion between hematite and magnetite and is accepted as an indication of a retrograde stage (Ciobanu and Cook, 2004). At this texture, magnetite overgrowth on the hematite margin is an indication of progressive destruction of prograde assemblage. Garnet and magnetite in the prograde assemblages also preserve evidence of retrograde textures. Pressure fluid-assisted brecciation is characteristically recognized in the garnet (Fig. 4i) and magnetite grains (Fig. 4j).

Quartz, calcite and some hydrous minerals such as epidote, tremolite, actinolite and chlorite are other constitutes of skarn mineralogy. Quartz of three different stages was observed in the skarn zones. The first stage is distinct from the others due to the absence of magnetite ore and the textures of prograde silica infiltration cherts in carbonates (Fig. 3l). The second stage is characterized by the magnetite ore, and this quartz is also accompanied by epidote and calcite, (Fig. 4h). The third stage, on the other hand, was observed in the brecciated host rock. Calcite on the mineral paragenesis described two different stages. The first stage accompanies garnet minerals in the magnetite-free samples and was also observed around silica infiltration chert in skarn carbonates (Fig. 3l), while the second stage accompanies magnetite ore. Epidote is abundant in the field and occurs in two different stages. The first stage accompanies magnetite ore with rhythmically banded (Fig. 3h) and nodular forms of characteristic prograde texture. However, a distinct lack of garnet in this type of epidotes indicates that this type belongs to the end of the prograde stages. On the other hand, second-stage epidote was observed with breccia-filling-type in the host rock. Minor amounts of magnetite, tremolite, actinolite and chlorite are also relatively sparse in the thin sections and accompany this second-stage epidote (Fig. 4l). Considering the geological and mineralogical properties, the mineral paragenesis and succession of the Sivrikaya skarn is determined as shown in Fig. 5.

3. Analytical techniques

Microthermometric measurements of the fluid inclusions were performed on double-polished wafers using a Linkam THMS-600 stage mounted on an Olympus BX51 microscope at the Department of Geological Engineering of Recep Tayyip Erdoğan University, Rize,

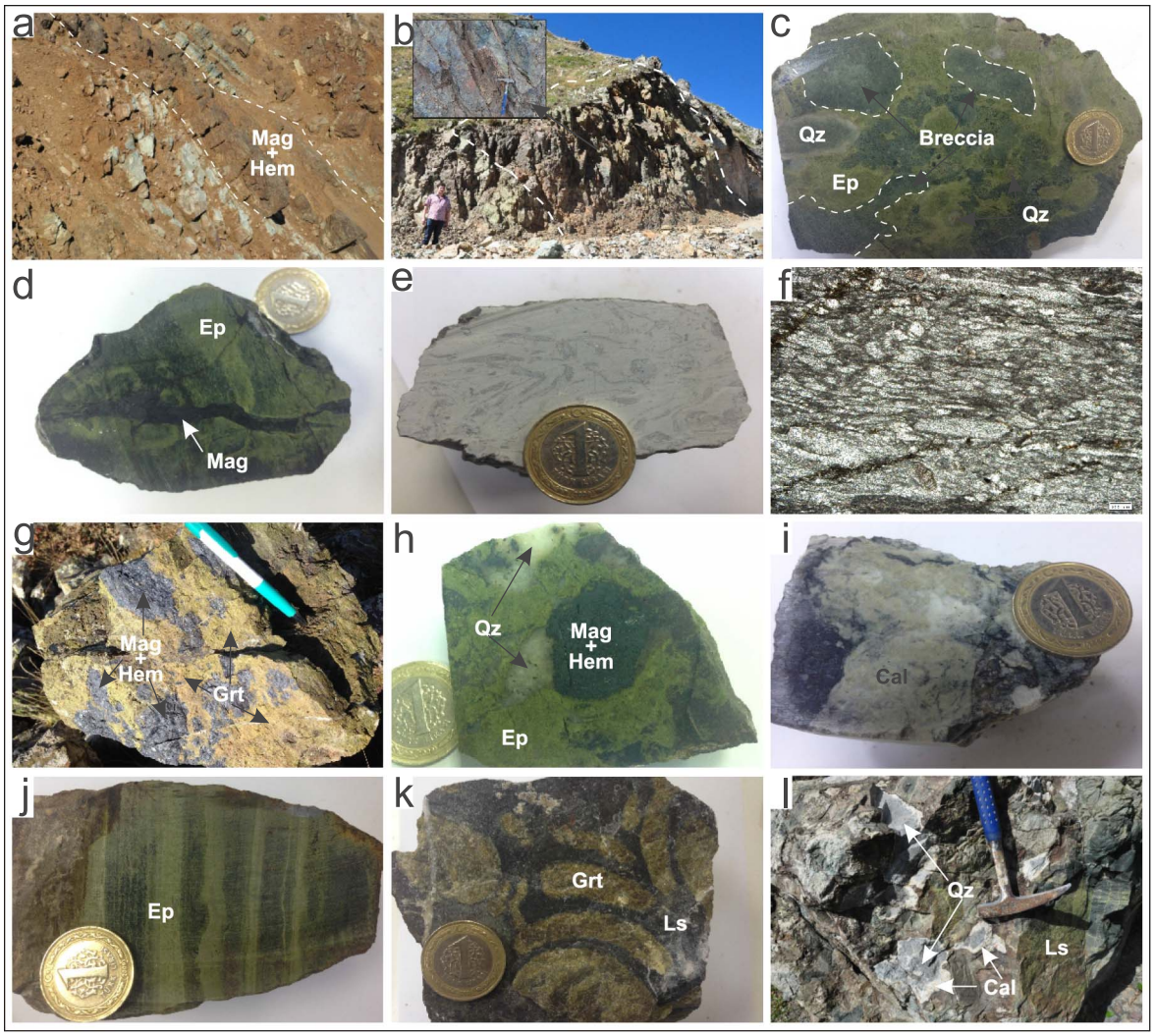

Fig. 3. a) Banded iron ore along the carbonate layer in volcano-sedimentary units; b) discontinuous ore pockets; c) breccia-filling-type epidote and quartz precipitation in volcanic host rocks along the skarn zone; d) fracture-filling-type, retrograde-stage magnetite; e) and f) macroscopic and microscopic view of organic material in the skarn carbonates; g) sporadically nodular magnetite and hematite assemblages within garnet; h) nodular iron oxides accompanying epidote and quartz; i) mossy texture of magnetite in light-colored carbonates; j) rhythmic intergrowth of magnetite and epidote; k) nodule-shaped reaction front of garnet aggregates from the carbonate skarn contact; l) silica infiltration chert in skarn carbonates (Abbreviations used in all figures and tables are according to Whitney and Evans, 2010.)

Turkey. Liquid nitrogen was used for freezing. The investigations were conducted within the temperature range of −196 °C to 600 °C. The measurement accuracy was ± 0.2 °C for the freezing experiment and ± 0.5 °C for the heating experiments for all types of fluid inclusions. The fluid inclusions were analyzed following the procedures described by Shepherd et al. (1985). Salinity values were calculated using the melting temperature of the last ice crystal (Potter et al., 1978).

The compositions of skarn minerals were analyzed using a Cameca SX-100 wavelength dispersive electron probe micro analyzer (EPMA) at the Department of Earth and Environmental Science at Ludwig Maximilian University in Munich, Germany. The operating conditions were 15–20 kV accelerating voltage, 20 nA beam current at a beam diameter of 1 μm and counting times of 20 s per element. Calibrations were performed using natural and synthetic reference materials of wollastonite for Ca and Si, orthoclase for Al and K, albite for Na, periclase for Mg, ilmenite for Ti and Mn, vanadinite for V, chromite for Cr, NiO for Ni, pure Co for Co and Fe_2O_3 for Fe. The Kα X-ray lines were used for each of the elements (Na, Mg, Al, Si, K, Ca, Ti, V, Fe, Cr, Mn, Co and Ni).

Carbon and Oxygen isotope analyses were completed at the Actlabs laboratory, Canada, by using an ion source VG SIRA-10 mass spectrometer. Approximately 2–5 mg of powdered calcite sample reacts with anhydrous phosphoric acid at 25 °C to produce CO_2. The evolved CO_2 gas was introduced into the isotope ratio mass spectrometer and analyzed for the $^{13}C/^{12}C$ ratio. The analytical precision using this technique is typically better than 0.2‰. Carbon and oxygen isotope compositions are reported relative to the international PDB (Pee Dee Belemnite) standards. The empirical relationship ($\Delta^{18}O_{SMOW} = 1.03086 - \Delta^{18}O_{PDB} + 30.86$) given by Friedman and Oneil (1977) was used for the conversion of the PDB standard to the SMOW standard.

Raman spectroscopic measurements were performed using Alpha 300 Confocal Raman Spectrometry at the Witec GmbH Ulm/Germany. The excitation wavelength was provided by a 520 nm (green) laser. The detector was an electronically-cooled open electrode (CCD). Data were collected over the spectral range 100–4000 cm^{-1} using 100X objective. The whole area, in different types of fluid inclusions, was scanned focusing the laser spot at 1 μm intervals.

4. Chemistry of skarn minerals

The composition of garnet and pyroxenes, considered the main skarn minerals, has special significance to classification of skarn type

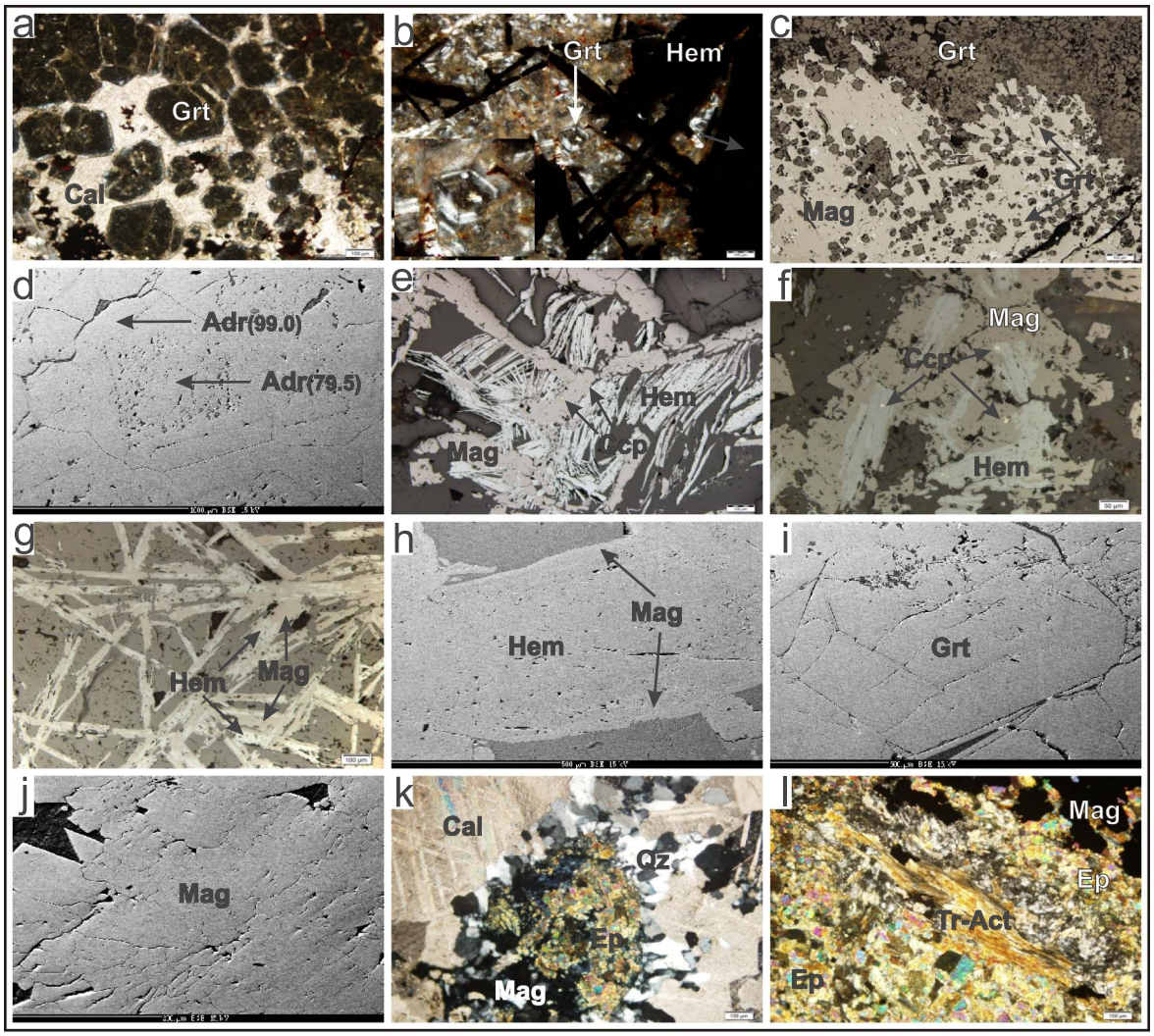

Fig. 4. a) Euhedral to subhedral coarse-grained garnet crystals in iron-free carbonates; b) fine-grained garnets accompanying iron ore and showing oscillatory zoning; c) coarsening of magnetite towards the boundaries with garnet; d) BSE images of oscillatory zoning in euhedral garnet in iron-free carbonates; e) needle-shaped oriented hematites cut by later-stage magnetites; f) chalcopyrite inclusions in magnetite and hematites; g) overgrowth of magnetite at the margin of hematite laths; h) BSE images of magnetite overgrowth on hematites; i) BSE images of retrograde brecciation of garnet; j) BSE images of retrograde brecciation of magnetite; k) quartz and epidote assemblages in the skarn carbonates; l) tremolite, actinolite and epidote accompanies to iron ore.

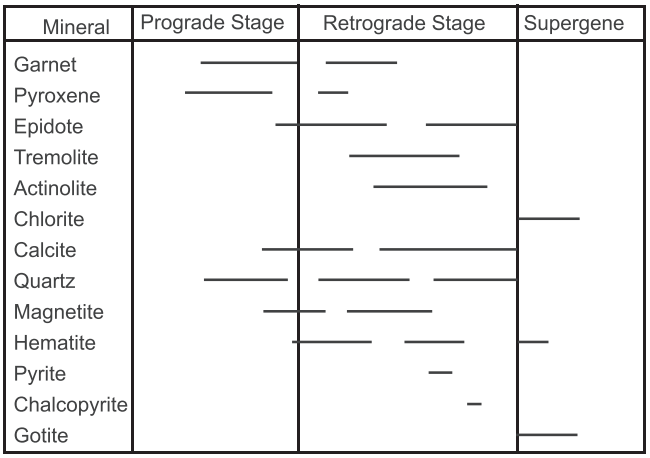

Fig. 5. Paragenetic diagram showing mineralization stages in the Sivrikaya skarn mineralization.

and in determining redox conditions because this type of deposit shows significant difference in geochemical and mineralogical aspect (Einaudi et al., 1981; Meinert, 1983, 1992). Einaudi et al. (1981) and Meinert, 1983, 1992 have indicated a close relationship between the metal content of skarn deposits and garnet and pyroxene compositions (Fig. 6a). Due to the particular importance of garnet and pyroxene, special attention has been given to their composition in this study.

4.1. Garnet

End-member calculations of garnets are given in Table 1 and graphically presented in Figure 6b together with garnet from other Fe-skarn deposits in the region. Chemical compositions of individual garnet grains from three different locations (Gölyayla, Meşebaşı and Kabahorn) are measured in the range of $Adr_{99.03}Grs_{0}Sps + Alm_{0.97}$ and $Adr_{88.04}Grs_{10.27}Sps + Alm_{1.69}$. No significant difference was detected in the composition of garnet grains from different locations. These results indicate that all the garnet grains are andradite-rich. The MnO content of these garnet grains never exceeds 0.66 wt%. Depending on lower MnO content, end-member calculations are always lower than 2% for spessartine. The higher andradite (Fe^{3+}) and lower spessartine (Mn^{2+}) content of the garnet minerals in the study area indicates oxidized skarn

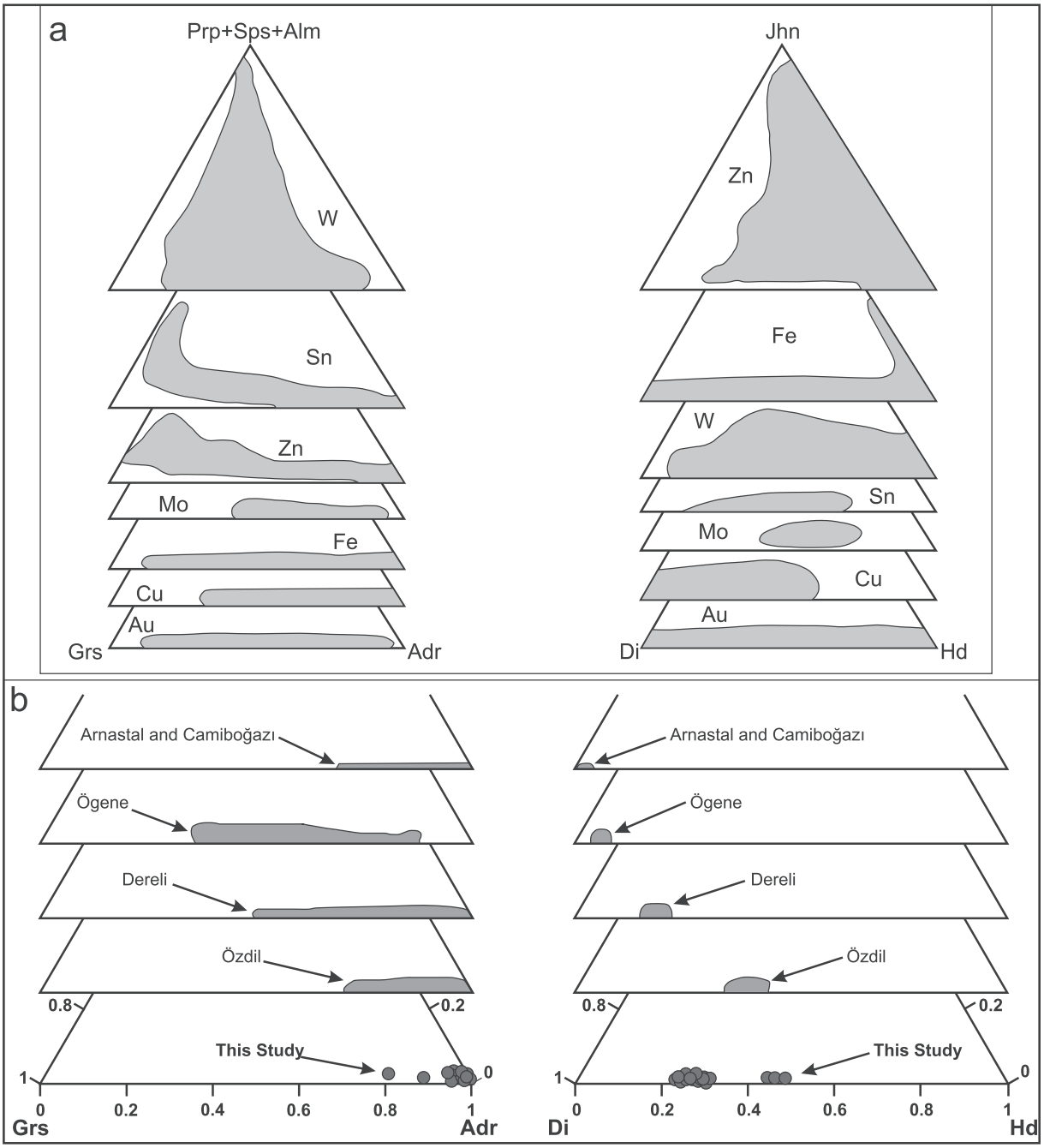

Fig. 6. a) Ternary plots of garnet and pyroxene compositions and related skarn-type deposits (Meinert, 1992); b) comparison of garnet and pyroxene composition with those from mostly known skarn deposits of northeastern Turkey (References for each skarn location are given in Table 5.)

type, according to Einaudi et al. (1981). Similarly, this type of andradite dominated garnet with a lower Mn content is also reported in the region by Sadıklar (1993), Saraç (2003) and Sipahi (2011).

In addition to single-point measurements, profile analyses were also performed on the oscillatory-zoned crystals. Decreasing Al_2O_3 content was observed in these profile analyses from core to rim, whereas FeO content increases. This zonation shows that garnet cores are more grossularitic than garnet rims. However, it should be noted that the highest grossular content in the core never exceeds $Adr_{79.45}Grs_{17.90}Sps + Alm_{2.65}$. This result indicates that andradite ratios are higher than grossular, even in the mineral core. This andradite-rich garnet composition in the core further increases towards the rim.

4.2. Pyroxene

Chemical analyses of clinopyroxene from the Sivrikaya skarn mineralizations are given in Table 2 and plotted in Figure 6b together with other Fe-skarn deposits in the region. Clinopyroxene from Sivrikaya Fe-skarn mineralizations formed under two different chemical compositions. The first group is associated with magnetite ore in the proximal zone, and the second group is accompanied by a magnetite-free distal zone. Clinopyroxene compositions in the magnetite ore predominantly fall in the diopside ($Di_{69.1-77.1}Hd_{22.2-29.8}Jhn_{0.6-1.4}$) area, whereas clinopyroxene in the magnetite-free zone falls in the intermediate ($Di_{49.8-54.0}Hd_{44.5-48.7}Jhn_{1.5-1.6}$) area (Fig. 6).

Mn/Fe ratio of these clinopyroxenes ranges from 0.04 to 0.10, which is quite compatible with other W-skarn deposits (Nakano et al.,

Table 1
Representative electron microprobe analyses of garnets from Sivrikaya Fe-skarn mineralization.

Sample	9/3	9/4	9/10	10/1	14/7	14/15	13/5	13/6	13/7	13/9	13/12	13/14
SiO_2	35.03	35.05	35.49	35.00	35.01	35.24	34.79	34.87	34.67	34.90	34.78	35.11
TiO_2	bdl	0.05	bdl	bdl	bdl	bdl	bdl	0.01	0.11	0.02	0.01	bdl
Al_2O_3	0.54	0.51	0.11	0.16	0.46	0.21	2.04	2.02	2.01	0.61	0.36	0.10
Cr_2O_3	bdl	bdl	bdl	bdl	bdl	0.03	bdl	bdl	bdl	bdl	bdl	0.02
Fe_2O_3	24.75	24.82	25.30	25.36	24.81	25.14	23.01	23.40	23.26	24.66	24.93	24.90
FeO	5.02	5.00	4.95	5.09	5.37	5.50	4.41	4.74	4.61	5.07	5.05	5.03
MnO	0.48	0.56	0.43	0.37	0.56	0.45	0.55	0.66	0.55	0.64	0.49	0.40
MgO	0.02	0.03	0.01	bdl	bdl	0.02	bdl	bdl	bdl	0.01	bdl	0.02
NiO	bdl	bdl	bdl	bdl	0.01	bdl	0.05	0.04	0.02	0.01	bdl	bdl
CaO	33.63	33.64	34.01	33.89	33.27	33.43	33.72	33.77	33.79	33.39	33.52	33.44
Total	99.47	99.67	100.30	99.87	99.50	100.03	98.57	99.51	99.03	99.32	99.15	99.03
Number of cation on the basis of 12 oxygen												
Si	3.011	3.008	3.027	3.005	3.012	3.018	2.993	2.978	2.975	3.006	3.004	3.032
Ti	bdl	0.003	bdl	bdl	bdl	bdl	bdl	0.001	0.007	0.001	0.000	bdl
Al	0.058	0.056	0.011	0.017	0.050	0.023	0.220	0.217	0.217	0.066	0.040	0.011
Cr	bdl	bdl	bdl	bdl	bdl	0.002	bdl	bdl	bdl	bdl	bdl	0.002
Fe^{3+}	1.601	1.603	1.624	1.638	1.606	1.621	1.490	1.504	1.502	1.598	1.621	1.618
Fe^{2+}	0.361	0.358	0.353	0.366	0.386	0.394	0.317	0.339	0.331	0.365	0.365	0.363
Mn	0.035	0.041	0.031	0.027	0.041	0.033	0.040	0.048	0.040	0.047	0.036	0.030
Mg	0.002	0.004	0.001	bdl	bdl	0.003	bdl	bdl	bdl	0.002	bdl	0.002
Ni	bdl	bdl	bdl	bdl	0.001	bdl	0.004	0.003	0.001	0.001	bdl	bdl
Ca	3.097	3.092	3.108	3.117	3.067	3.068	3.108	3.091	3.106	3.081	3.103	3.094
Total	8.165	8.165	8.156	8.170	8.165	8.161	8.172	8.181	8.179	8.167	8.169	8.153
Andradite	96.71	96.85	99.34	99.03	97.15	98.58	87.83	88.08	88.08	96.27	97.77	99.28
Grossular	1.80	1.35	0.00	0.00	1.16	0.00	10.60	10.06	10.35	1.78	0.78	0.00
Prp + Sps + Alm	1.49	1.80	0.66	0.97	1.69	1.42	1.57	1.86	1.57	1.95	1.46	0.72

bdl: below detection limit.

Table 2
Representative electron microprobe analyses of clinopyroxenes from the Sivrikaya Fe-skarn mineralization.

Sample	S37-14	S37-1	S37-5	S37-9	S37-20	S36-3	S36-6	S36-14	S36-17	36-4	S36-5	S36-6
SiO_2	51.80	51.10	51.28	49.98	51.26	51.87	51.36	51.44	52.23	50.00	49.26	50.60
TiO_2	0.54	0.50	0.49	0.52	0.52	0.37	0.55	0.45	0.36	0.52	0.72	0.46
Al_2O_3	1.82	2.08	2.05	2.75	1.92	2.31	2.26	2.45	2.30	3.56	3.69	3.34
Cr_2O_3	0.03	bdl	0.06	0.03	0.07	0.14	bdl	0.08	0.07	0.05	0.01	0.05
FeO[a]	11.22	9.55	10.07	10.56	10.72	8.14	10.21	8.99	8.13	18.98	19.95	18.52
MnO	0.44	0.34	0.37	0.51	0.40	0.31	0.35	0.29	0.24	0.66	0.59	0.65
MgO	14.69	15.79	15.29	14.66	14.96	15.64	14.99	15.48	15.77	12.17	11.31	12.59
CaO	19.60	20.10	19.49	19.98	19.69	21.00	19.36	20.22	20.68	9.99	10.26	9.89
Na_2O	0.26	0.27	0.30	0.29	0.29	0.22	0.29	0.27	0.23	1.49	1.77	1.35
K_2O	bdl	bdl	0.01	0.01	bdl	0.01	bdl	0.01	bdl	0.33	0.57	0.30
Total	100.44	99.79	99.49	99.33	99.93	100.07	99.40	99.73	100.03	97.81	98.21	97.78
Number of cation on the basis of 6 oxygen												
Si	1.936	1.913	1.927	1.893	1.925	1.925	1.929	1.920	1.934	1.947	1.929	1.962
Ti	0.015	0.014	0.014	0.015	0.015	0.010	0.016	0.013	0.010	0.015	0.021	0.013
Al	0.080	0.092	0.091	0.123	0.085	0.101	0.100	0.108	0.100	0.163	0.170	0.153
Cr	0.001	bdl	0.002	0.001	0.002	0.004	bdl	0.002	0.002	0.002	0.000	0.002
Fe	0.349	0.296	0.314	0.331	0.334	0.251	0.319	0.279	0.251	0.615	0.646	0.599
Mn	0.014	0.011	0.012	0.016	0.013	0.010	0.011	0.009	0.008	0.022	0.020	0.021
Mg	0.818	0.881	0.856	0.828	0.838	0.866	0.839	0.861	0.871	0.707	0.660	0.728
Ca	0.785	0.806	0.784	0.811	0.792	0.835	0.779	0.809	0.820	0.417	0.430	0.411
Na	0.019	0.020	0.022	0.021	0.021	0.016	0.021	0.020	0.017	0.112	0.134	0.102
K	bdl	bdl	0.000	0.000	bdl	0.000	bdl	0.000	bdl	0.016	0.028	0.015
Total	4.017	4.034	4.023	4.038	4.025	4.019	4.014	4.021	4.012	4.016	4.039	4.005
%Jhn	1.17	0.91	0.99	1.40	1.08	0.88	0.96	0.81	0.67	1.63	1.48	1.59
%Hd	29.56	24.94	26.59	28.16	28.22	22.31	27.30	24.28	22.22	45.78	48.71	44.45
%Di	69.27	74.15	72.43	70.44	70.70	76.82	71.75	74.92	77.11	52.60	49.81	53.96

[a] Total iron as FeO; bdl: below detection limit.

1994, Nakano, 1998). These clinopyroxene compositions are also compatible with clinopyroxene from Özdil (Sadıklar, 1993), Kotana and Ögene (Saraç, 2003) and Camiboğazı (Sipahi, 2011), Fe-skarn deposits in the close proximity to the study area.

5. Fluid inclusion studies

Fluid inclusion measurements were performed on quartz, calcite, garnet and epidote minerals, which are closely associated with the skarn. Before freezing–heating experiments, fluid inclusion types were petrographically determined in each crystal. Primary, secondary and pseudo-secondary fluid inclusions were identified in the double-polished wafers using the criteria of Roedder (1984) and Van den Kerkhof and Hein (2001). Microthermometric measurements were carried out only on the primary inclusions due to possible post mineralization effects on the mining environment.

Fluid inclusions were extensively observed in the quartz and calcite, while a limited number of inclusions were available in garnet and epidote minerals. The size of investigated fluid inclusions varied between 8 and 30 μm with the exception of several inclusions larger than 50 μm. Most of the fluid inclusions occurred in irregular shapes. Lesser amounts of circular, elliptical, pear-shaped and tube-shaped inclusions were also present. Exceptionally, some inclusions in calcite minerals are tabular in shape, in accordance with the rhombohedral system of the host crystal. Most of the inclusions had two phases (liquid + vapor), while single-phase (liquid- or vapor-bearing) inclusions were less commonly observed. Microthermometric measurements were carried out on two-phase inclusions due to unavailable phase transitions in single phases. None of the inclusions were found to contain daughter phase or liquid CO_2 at room temperatures.

Two types of fluid inclusions were classified in the liquid- and vapor-bearing two-phase inclusions. The first type of inclusions is two-phase liquid and vapor (L + V) inclusions, and vapor ratios are lower than unity (V < L). Homogenization to liquid phase by the disappearance of vapor occurs in this type of inclusion, and this type was observed in all the investigated minerals of different stages. No decisive diversity was identified in these types of inclusions in different-stage minerals in terms of inclusion shape and size; the main differences were the vapor/liquid ratios at room temperature. Vapor/liquid ratios of type I inclusions in first-stage garnet (Fig. 7a) and quartz (Fig. 7e) are ~30–40%, while this ratio is ~20–30% in the second-stage garnet (Fig. 7b) and quartz (Fig. 7f). Similar ratios in early-stage epidote (Fig. 7c) and calcite (Fig. 7h) were measured because second-stage garnet and quartz correspond to the early-stage epidote and calcite in the mineral paragenesis (Fig. 5). Second-stage epidote (Fig. 7d) and calcite (Fig.7i) are characterized by volumetrically smaller ratios (V < 20%). Vapor/liquid ratios of third-stage quartz (Fig. 7g) are also lower than 10%.

On the other hand, type II inclusions are two-phase, possessing liquid and vapor phases (L + V), whereas vapor ratios are higher than unity (V > L). Homogenization to vapor phase occurs in these types of inclusions. Type I inclusions were observed in different stages of all the investigated minerals. Type II inclusions, however, were identified only in the early-stage quartz. According to this explanation, type II inclusions accompany type I inclusions in early-stage quartz, even in the same minerals (Fig. 7e). Homogenization to liquid phase was observed in type I inclusions, whereas type II inclusions homogenize to vapor phase.

5.1. Eutectic temperature (Te) measurements

The eutectic temperatures (Te) have been measured in all types and stages of inclusions in garnet, epidote, quartz and calcite minerals. The eutectic temperatures of the early-stage type I inclusions in garnet and quartz as well as type II inclusions in the same-stage quartz are measured in the range of −40.8 to −53.6 °C (Fig. 8). These data are very close to eutectic temperatures of H_2O–$CaCl_2$ systems (−49.5 °C) (Shepherd et al., 1985; Wilkinson, 2001). In constrast, the eutectic temperatures of the first-stage fluid inclusions in epidote and calcite are higher (up to −31.8 °C), which corresponds to the H_2O–$MgCl_2$ system in this type of inclusion.

The eutectic temperature of first-stage inclusions in garnet is

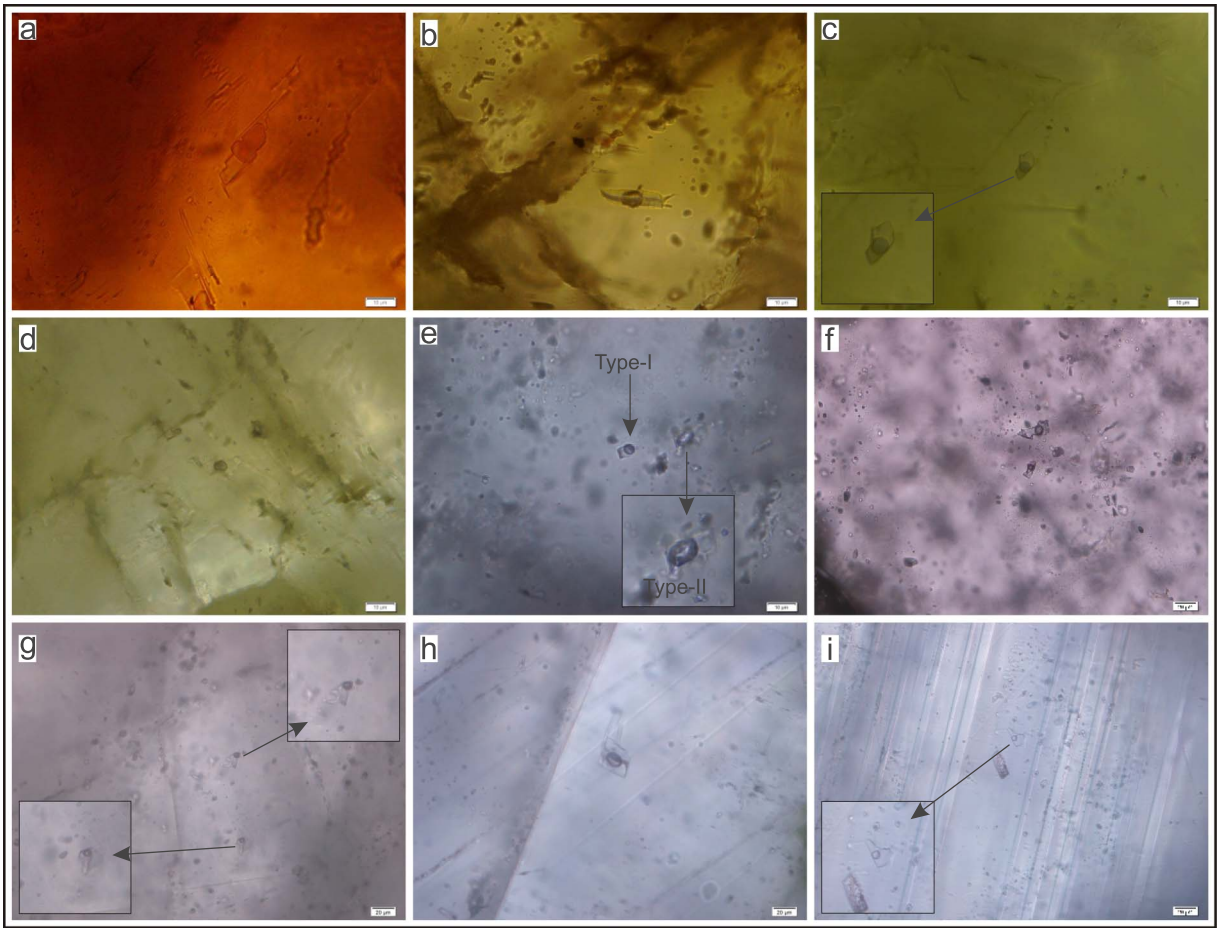

Fig. 7. Photomicrographs of primary fluid inclusions in different minerals: Liquid-rich type I fluid inclusions in first (a) and second (b) stage garnet minerals; liquid-rich type I fluid inclusions in early (c) and late (d) stage epidote minerals; liquid-rich (type I) and vapor-rich (type II) fluid inclusions in first stage quartz minerals (e); liquid-rich type I fluid inclusions in second-stage (f) and stage 3 (g) quartz minerals; liquid-rich type I fluid inclusions in first- (h) and second-stage (i) calcite minerals.

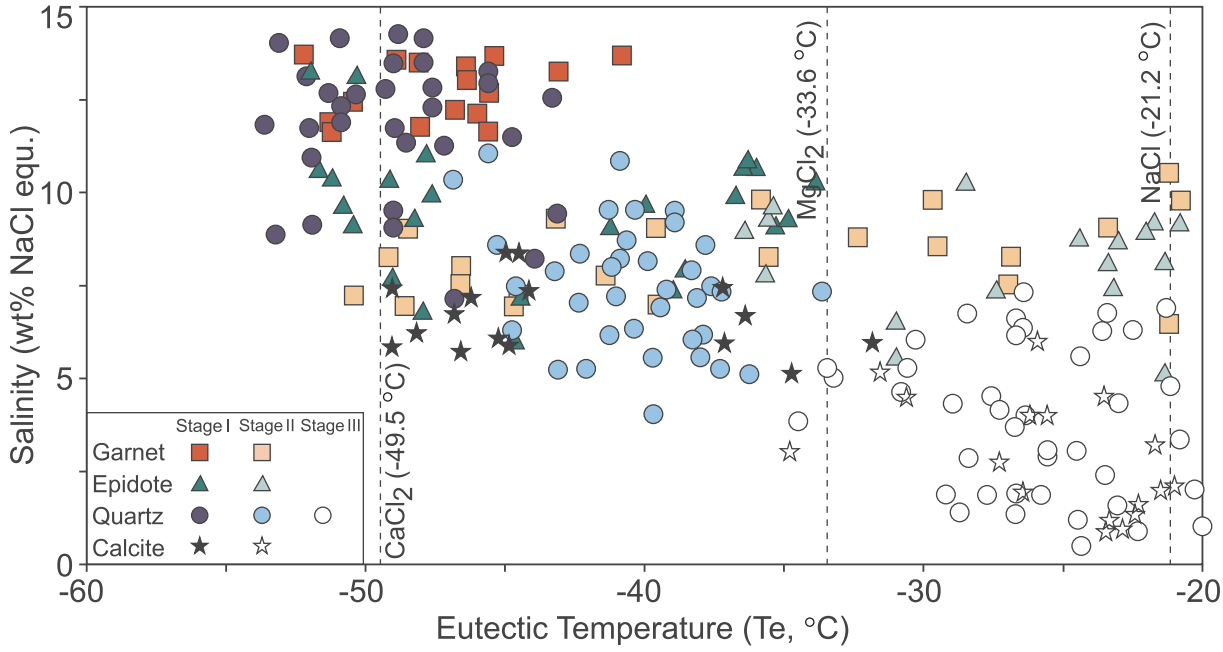

Fig. 8. Comparison of measured eutectic temperatures of fluid inclusions from different stages of mineral phases with eutectic temperatures of specific salt solutions.

scattered over a wide temperature range between −50.4 °C and −20.8 °C. This range corresponds to the mixture of H_2O–$CaCl_2$–$MgCl_2$–KCl–$NaCl_2$ water salt systems rather than the specific eutectic temperature of single phases. Eutectic temperatures of second stage inclusions in epidote and calcite are scattered in narrow ranges between −20.8 °C and −36.6 °C, corresponding to a mixture of $MgCl_2$- and $NaCl_2$-type salt in the inclusions. However, slightly lower eutectic temperatures in second stage inclusions of quartz, with values between −45.3 °C and −33.4 °C, correspond to a mixture of $CaCl_2$ and $MgCl_2$ in the system. Finally, eutectic temperatures of third stage inclusions in quartz are very close to the eutectic temperature of the H_2O–NaCl system (Shepherd et al., 1985). Considering eutectic temperatures of all stages of inclusions, the composition of early stages was characterized by the $CaCl_2$-dominated system. The compositions become NaCl-dominated in later stages.

5.2. Ice melting temperature (Tm–ice) measurements

Final ice melting (Tm–ice) temperatures were measured in different stages of fluid inclusions in all investigated minerals. Corresponding salinity content of Tm–ice values was calculated as wt% NaCl equivalent in accordance with the equation of Bodnar (1993). Tm–ice values of fluid inclusions from each mineral and corresponding salinity values are given in Table 3 and plotted in Figure 9.

Tm–ice values of first-stage fluid inclusions in garnet and quartz (including type II inclusions in quartz) were measured between −3.7 °C and −10.1 °C. The salinity content of these fluid inclusions was calculated between 6.0 and 14.3 wt% NaCl equivalent. Tm–ice values of second stage inclusions in garnet and quartz minerals were measured in the range of −3.1 °C to −6.9 °C. The salinity content of these inclusions was also calculated between 5.1 and 10.5 wt% NaCl equ. Very close salinity values were calculated for the first- and second-stage fluid inclusions in epidote minerals in the range of 6.0–13.3 wt% NaCl equ. and 5.1–10.5 wt% NaCl equ., respectively. In constrast, the lower salinity content of the second-stage fluid inclusions in calcite was clearly distinguished (between 6 and 8.1 wt% NaCl equ.) compared to the early-stage values (between 0.7 and 6.3 wt% NaCl equ.). In addition, the salinity content of the third-stage inclusions (observed in quartz minerals) was also calculated in the range of 0.5–8.88 wt% NaCl equ., according to measured Tm–ice values between −0.3 °C and −5.7 °C.

The salinity contents of all fluid inclusions are in the range of 0.5–14.3 wt% NaCl equ. The salinity content of inclusions at each stage comprises different populations (Fig. 9). The early stage inclusions demonstrate higher T_h and salinity, whereas the later stages show lower T_h and salinity values. Decreasing salinity content of the fluid inclusions with decreasing T_h values was determined in the fluid inclusions of all investigated minerals.

5.3. Homogenization temperature (T_h) measurements

The results of measured homogenization temperatures of each stage of fluid inclusions in different minerals are presented in Table 3. Homogenization temperatures of two different stages of fluid inclusions in garnet and calcite were measured in the range of 352–436 °C and 174–368 °C, respectively. The T_h frequency histogram indicates that mineralization of garnet occurred at relatively high temperatures, whereas calcite minerals occurred at lower temperature conditions (Fig. 10). Although two types of fluid inclusions are determined in each mineral, the T_h frequency histogram of both garnet and calcite is represented by a unimodal distribution (single-peaked histogram) due to the overlap of the data. Homogenization temperatures of three different stages of fluid inclusions in quartz were measured between 166 °C and 462 °C, and this temperature ranges between 256 °C and 422 °C in two different stages of fluid inclusions in epidote minerals. Three different stages of inclusions in quartz, and two different stages of inclusions in epidote, are clearly described with triple- and double-peaked histograms, respectively (Fig. 10).

6. Raman studies

Fluid inclusions in all the studied minerals contain liquid and gas phases in different ratios. None of these inclusions were found to contain aqua CO_2 phases. Clathrate occurrences have not been observed during microthermometric measurements. This is an indication of the distinct lack of CO_2 gases. Nevertheless, representative inclusions of different types were measured using Raman spectroscopy to confirm if there are any other volatiles. These measurements were performed using area scanning, since there is no separated gas species in the fluid inclusions. The Raman analyses of second and third-stage inclusions showed that H_2O is the dominant component, and other comprehensive

Table 3
Microthermometric fluid inclusion data from Sivrikaya Fe-skarn mineralization.

Mineral	FI Type	FI Types	Homogeniz. modes	Statistical Parameters	Te (eutectic, °C)	Tm-ice (°C)	Salinity wt% NaCl equ.	Th, (°C)
Garnet	Type-I	Stage-I	Liquid	Max	−40.8	−7.9	13.8	436
				Min	−52.2	−9.7	11.7	378
				Mean	−47.3	−8.8	12.8	407
				n	16	22	22	23
		Stage-II	Liquid	Max	−20.8	−3.9	10.5	405
				Min	−50.4	−6.9	6.3	352
				Mean	−36.8	−4.6	7.4	377
				n	23	29	29	29
Epidote	Type-I	Stage-I	Liquid	Max	−35.4	−3.7	13.3	422
				Min	−51.9	−9.2	6.0	307
				Mean	−43.3	−6.5	10.0	378
				n	27	41	41	46
		Stage-II	Liquid	Max	−20.8	−3.1	10.5	382
				Min	−36.6	−6.9	5.1	256
				Mean	−28.7	−5.4	8.5	319
				n	17	35	35	36
Calcite	Type-I	Stage-I	Liquid	Max	−31.8	−3.7	8.1	368
				Min	−50.4	−5.1	6.0	268
				Mean	−43.7	−4.3	6.9	318
				n	16	33	33	31
		Stage-II	Liquid	Max	−21.1	−0.4	6.3	346
				Min	−36.4	−3.9	0.7	174
				Mean	−28.8	−2.1	3.5	288
				n	16	40	40	49
	Type-II	Stage-I	Vapor	Max	−44.2	−5.6	13.4	462
				Min	−52.9	−9.3	8.7	389
				Mean	−47.4	−7.7	10.3	412
				n	12	17	17	26
Quartz	Type-I	Stage-I	Liquid	Max	−43.1	−4.5	14.3	458
				Min	−53.6	−10.1	7.2	346
				Mean	−45.4	−6.6	10.1	396
				n	18	28	28	32
		Stage-II	Liquid	Max	−33.4	−3.1	10.5	397
				Min	−45.3	−6.9	5.1	240
				Mean	38.7	−4.8	7.6	334
				n	25	37	37	68
		Stage-III	Liquid	Max	−20.8	−0.3	8.9	324
				Min	−34.5	−5.7	0.5	166
				Mean	−26.2	−2.3	3.9	232
				n	47	52	52	72

volatiles are not present. However, first-stage inclusions in quartz (Fig. 11a), epidote (Fig. 11b) and garnet (Fig. 11c) were rarely found to contain organic compounds such as CH_4 and CH_2. Raman spectra of CH_4 showed only one peak at around 2917 cm^{-1}, whereas this band is around 1448 cm^{-1} for the CH_2 species (Atamas et al., 2004; Lin et al., 2007; Burke, 2001). These organic compounds were only detected in three of 22 measured inclusions. Additionally, fluid inclusions in calcite were also measured, but no decisive spectra were obtained due to higher fluorescence effects.

7. Carbon and oxygen isotope studies

Carbon and oxygen isotopic composition of dolomitic limestones and skarn calcite along the skarn zones was studied in two different locations to provide information about the origin of mineralizing fluids and the depositional environment of limestones (Bowman, 1998). The isotope analyses were conducted on 12 samples, and results are presented in Table 4 and plotted in Figure 12.

The $\delta^{13}C$ values of dolomitic limestones were measured in the range of −5.3‰ and −6.5‰ in the Gölyayla location, whereas these values were in the range of −1.8‰ and −2.35‰ in the Kabahorn location. The $\delta^{13}C$ values of skarn calcites are distinctly heavier than those of dolomitic limestones, ranging between 0.5‰ and −4.2‰ in the Gölyayla location and 0.7‰ and −1.4‰ in the Kabahorn locations.

The $\delta^{18}O$ values were measured between 10.9‰ and 12.45‰ in dolomitic limestones of the Gölyayla and Kabahorn locations. The $\delta^{18}O$ values of skarn calcites range between 7.61‰ and 9.78‰ in both locations. Dolomitic limestones show conspicuous depletion in $\delta^{18}O$ in both locations relative to typically reported $\delta^{18}O$ values of marine limestones (Taylor, 1976; Hoefs, 1987; Allegre, 2008) (Fig. 12). Skarn calcites are also further depleted in their $\delta^{18}O$ values. In the diagram (Fig. 12) of $\delta^{13}C_{PDB}$ vs. $\delta^{18}O_{SMOW}$, all the samples are plotted in the field between marine limestones and mantle-derived carbonatite, with a slope of negative correlation. This trend is consistent with the decarbonatization of organic material in Figure 12.

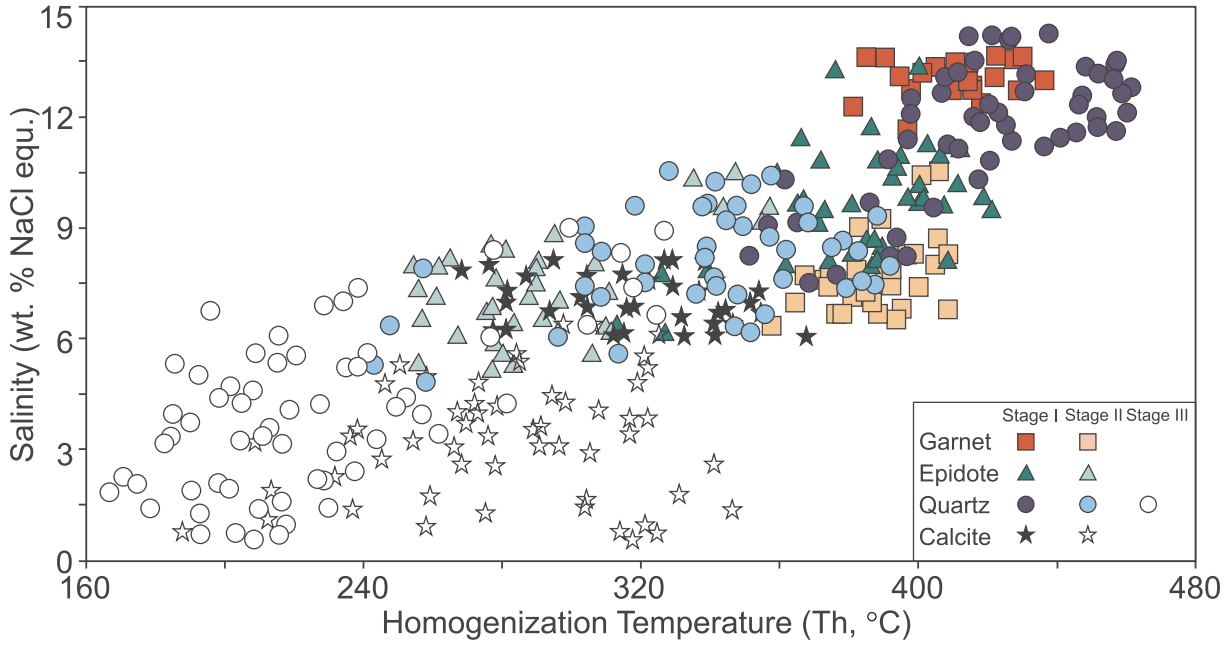

Fig. 9. Distribution of salinity content of the fluid inclusions versus T_h data in different stages of mineral phases.

8. Discussion

8.1. Skarn environment and textural properties

The Sivrikaya skarn mineralization was formed along the contact between İkizdere Granitoid and Late Cretaceous limestone and marble in the sedimentary layer of the volcanic-dominated Çatak Formation. Exoskarn-type mineralization was identified in the area, with a mineral paragenesis of andradite, diopside, epidote, tremolite, actinolite chlorite, quartz and calcite. Magnetite and hematite are the main ore minerals, containing limited amounts of pyrite and chalcopyrite inclusions.

Fracturing of andradite and magnetite were commonly observed under the microscope (Fig. 4i and j). Additionally, volcano-sedimentary host rock, accompanying the ore, commonly fractured (Fig. 3a) and brecciated the host rock (Fig. 3c) which is widespread along the skarn front. According to Yardley and Lioyd (1995) and Dipple and Gerdes (1998), this texture is indicative of changes in permeability–porosity at the skarn front and is a response to hydrofracturing and brecciation. They also indicated that possible contributions from meteoric waters in near-surface environments can cause boiling and collapse of the skarn system. Similar findings, reported by Shelton (1983), Clechenko and Valley (2003), and Meinert et al. (2005) also demonstrate that highly fractured and brecciated host rocks are an indication of shallow emplacement of granitic intrusion because increasing hydraulic pressure causes fractures in the overlying unit. Taking into account the above explanations, brecciated texture at the microscopic scale and highly brecciated host rocks are indicative of increasing permeability along near-surface skarnization. Such a shallow skarn environment indicates that not only magmatic solutions but also meteoric water are involved in the skarnization. The addition of meteoric water may also be an explanation for why hydrous minerals such as epidote, tremolite, actinolite and chlorite were dominant along the skarn zone.

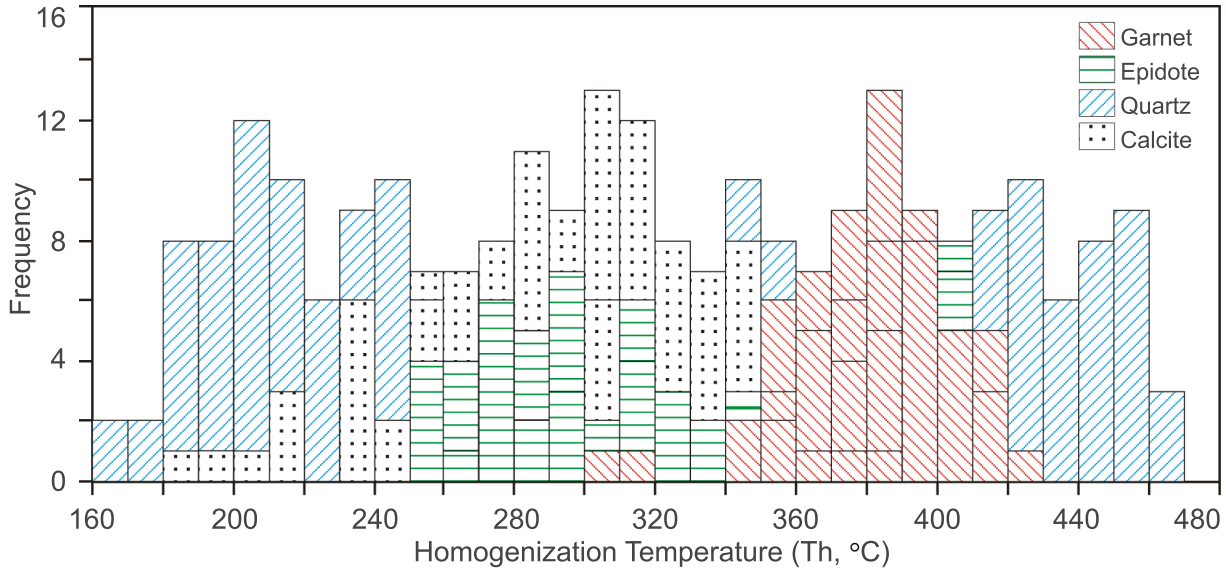

Fig. 10. Histograms of homogenization temperatures of fluid inclusions in garnet, epidote, calcite and quartz minerals.

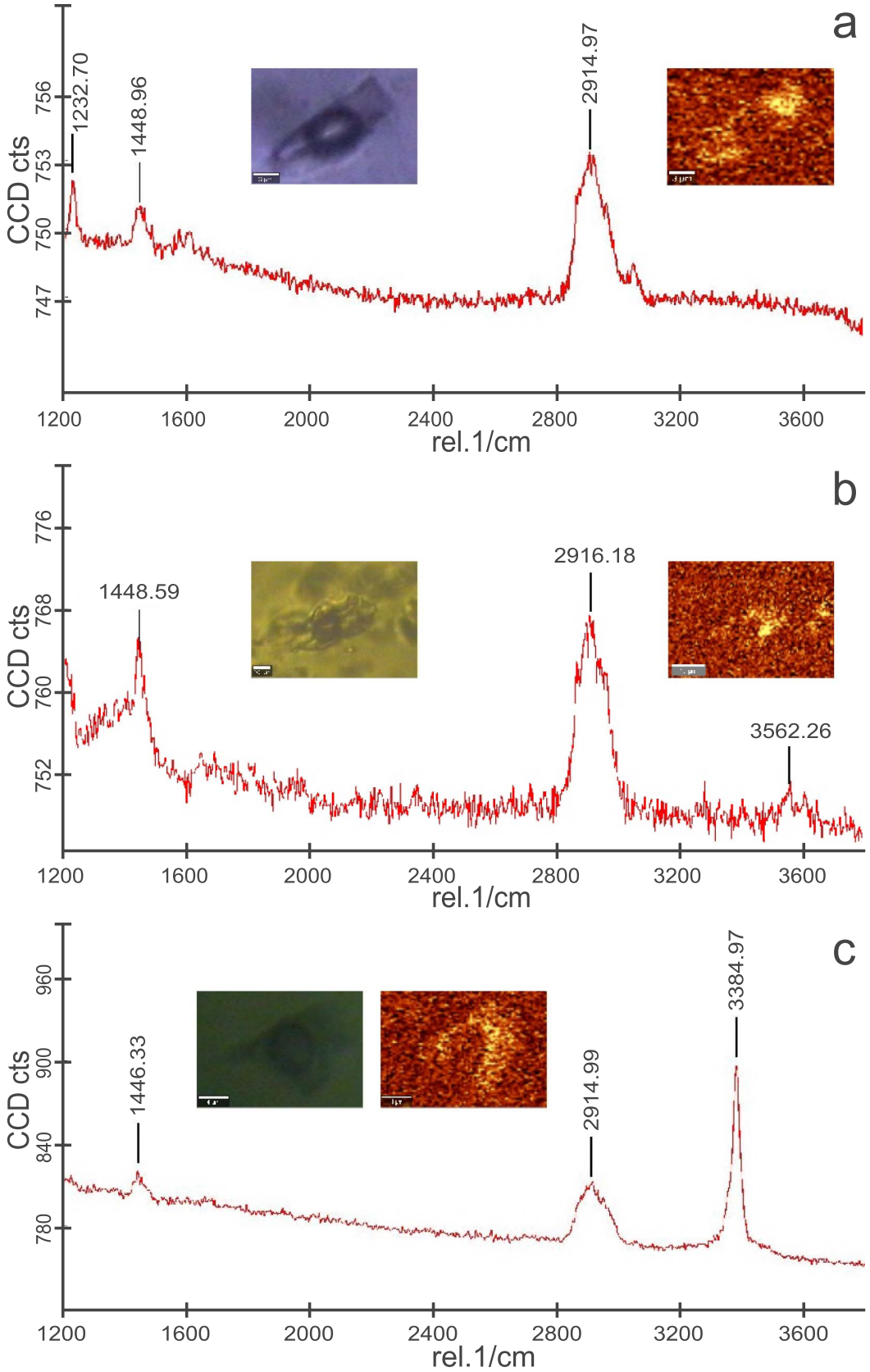

Fig. 11. Raman spectra of the CH_4 and CH_2 bearing fluid inclusions in quartz (a), garnet (b) and epidote (c) minerals.

Table 4
Carbon and oxygen isotopic compositions of skarn calcite and dolomitic limestones from the Sivrikaya Fe-skarn mineralization.

Location	Sample Type	Sample	$\delta^{13}C_{PDB}$	$\delta^{18}O_{PDB}$	$\delta^{18}O_{SMOW}$
Gölyayla	Skarn calcite	L2-3	−0.4	−21.9	8.3
		L10-3	0.5	−21.9	8.3
		S55	0.5	−22.3	7.9
		L4-3	−4.2	−22.6	7.6
	Dolomitic limestone	L1-1	−5.3	−19.5	10.8
		L4-2	−6.5	−18.8	11.5
Kabahorn	Skarn calcite	L2-1	−0.8	−20.5	9.8
		L2-2	−1.4	−21.3	9.0
		S8-2	0.7	−21.3	9.0
		L1-2	−1.3	−20.6	9.7
	Dolomitic limestone	L1-3	−1.8	−18.6	11.7
		L4-1	−2.4	−17.9	12.5

8.2. Host rock geochemical evidence for skarn type and environment

The relationship between major- and trace-element composition of igneous rocks and related skarn types has been investigated in pioneering studies (Newberry, 1987; Meinert, 1983; Meinert et al., 2005; Kwak and White, 1982). These studies concluded that in terms of major elements, most plutons associated with skarn deposits are fairly normal calc–alkaline, and in terms of Al saturation, most of them are close to the metaluminous feature (Meinert et al., 2005). The whole-rock geochemical analyses performed by Evcimen (2011) indicate that İkizdere plutonic rocks are metaluminous to slightly peraluminous with ASI [(molar $Al_2O_3/(CaO + K_2O + Na_2O)$] ranging from 0.86 to 1.04. Calc–alkaline and high-K calc–alkaline characters for these plutonic rocks are also determined by Evcimen (2011).

Comparing the trace element content of the İkizdere Pluton with other skarn-producing granitoides, high V content refers to the calcic Fe-skarns (Fig. 13a) because vanadium substitutes with the oxide phase (Meinert et al., 2005). The lower Rb/Sr ratio of the İkizdere Pluton is also closely associated with Fe-type skarn deposits (Fig. 13b). Based on the variation of Nb versus Y (Fig. 13c), and Rb versus Y + Nb (Fig. 13d) diagrams, İkizdere plutonic rocks are closely associated with volcanic arc-related granitoides, and this type of plutonic rock is always responsible for the formation of Fe-type skarn occurrences. According to the above explanations, in addition to major- and trace-element variations, volcanic arc-related features of İkizdere plutonic rocks are consistent with Fe-type skarn formations.

8.3. Classification of skarn types

Garnet and pyroxene compositions in skarns are particularly important because compositional variations can provide significant information on the skarn-forming environment and the classification of skarn types (Einaudi et al., 1981; Newberry, 1983; Meinert, 1992; Kwak, 1987). Kwak (1987), Newberry (1983) and Einaudi et al. (1981) indicated that andraditic garnet represents oxidized environments, whereas grossularitic garnet is an indication of reduced conditions. Authors including Meinert et al. (2005), Jamtveit (1991), Clechenko and Valley (2003) and Ciobanu and Cook (2004) have also indicated that increasing Adr/Grs ratios from core to rim in oscillatory-zoned garnet is an indication of increasing oxidizing conditions.

The diopside-rich end-member of pyroxenes from the Sivrikaya mineralization characterizes an oxidized skarn environment, according to early studies (Newberry, 1991; Nakano et al., 1994, 1998). Meinert et al. (2005) also indicated that abundance of garnet is more common than that of pyroxene in an oxidized skarn environment. According to the above explanations, occurrence of andradite ($Adr_{79.45-99.03}$), diopside ($Di_{69.1-77.1}$), increasing andradite ratios in zoned crystals, and greater abundances of garnet rather than pyroxene in the study area, indicate oxidized conditions.

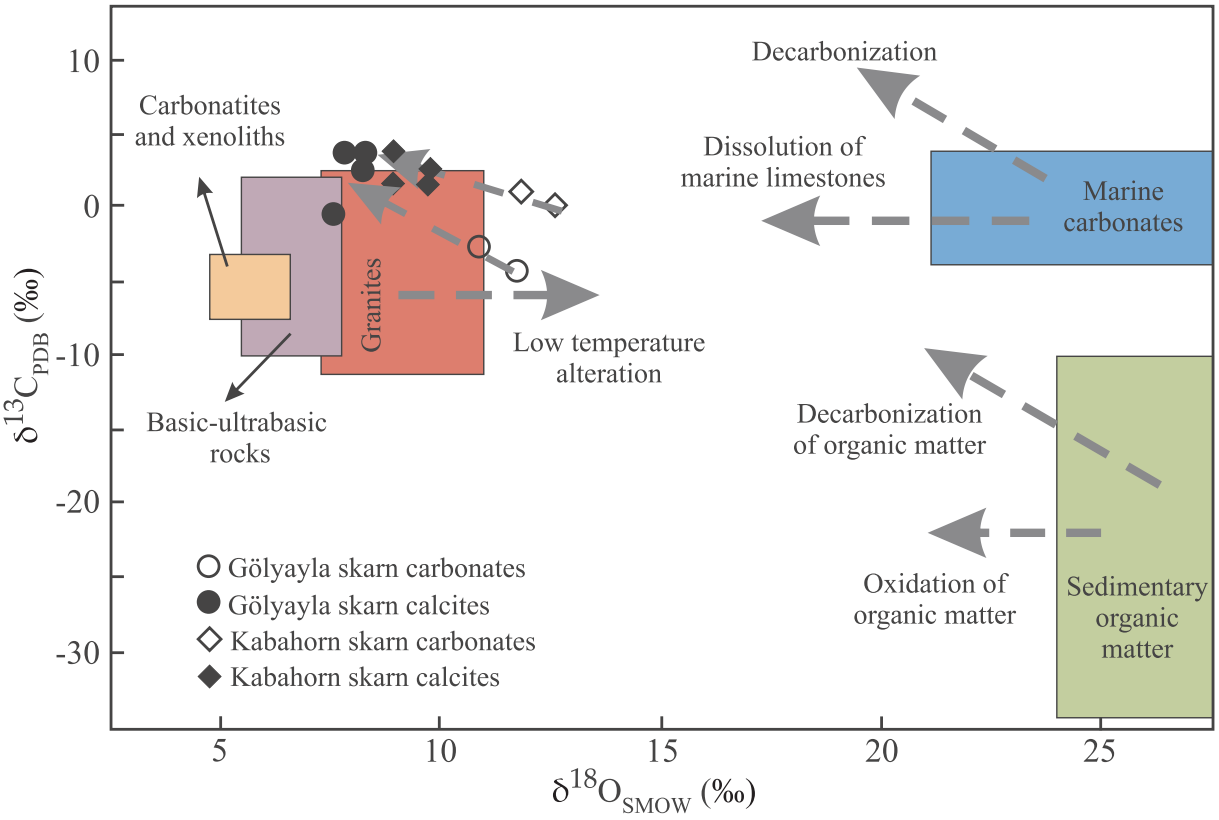

Fig. 12. Diagram of $\delta^{13}C_{PDB}$ vs. $\delta^{18}O_{SMOW}$ for the Sivrikaya skarn carbonates and calcites and comparison with the $\delta^{13}C$ and $\delta^{18}O$ isotope composition of mostly known rock types.

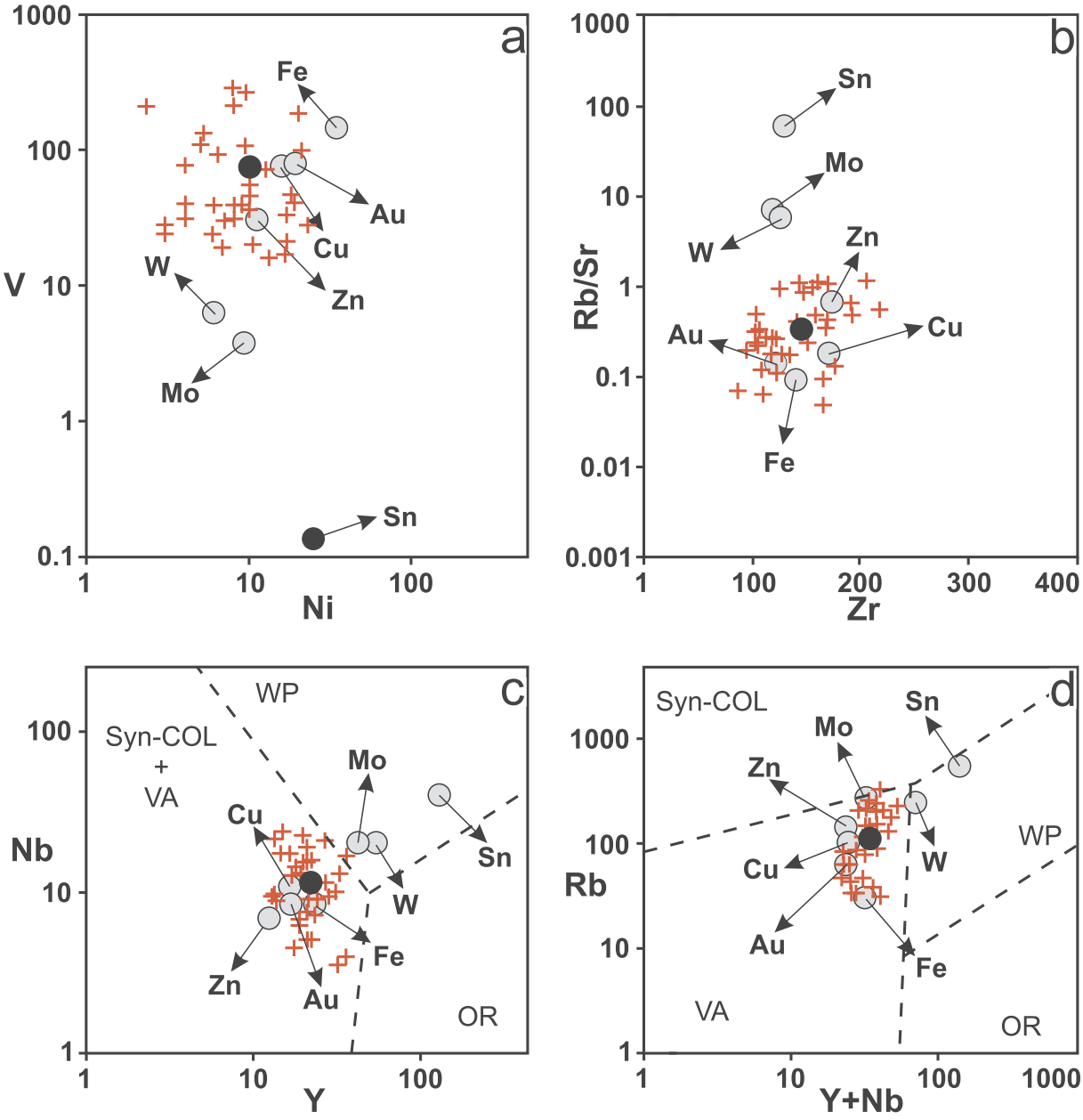

Fig. 13. a) Vanadium versus Ni and b) Rb/Sr ratio versus Zr discrimination diagrams; c) and d) tectonic settings trace-element discrimination diagrams for plutonic rocks associated with the main skarn deposit types (Syn–Col: syn–collision; VA: volcanic–arc; WP: within-plate; OR: ocean-ridge plutonic rocks). Raw data (cross) and mean values (black circle) from Evcimen (2011); other mean values (light grey circle) from Meinert et al. (2005).

Pyroxene composition in the proximal zone was found to be diopside-dominated, whereas the composition of pyroxenes hedenbergite dominated in the distal zone (Fig. 6b). This is quite compatible with the finding of Ciobanu and Cook (2004) that clinopyroxenes are Mg-rich (Di > 69) due to interaction with magnetite-rich ore in the proximal zone, whereas they are more diluted with hedenbergitic compositions in the distal zone.

The relationship between garnet and pyroxene composition and dominant metal content of the skarn deposit has been determined in previous investigations (Burt, 1972; Einaudi et al., 1981; Einaudi and Burt, 1982; Nakano et al., 1994). The andradite and diopside composition of the Sivrikaya mineralization is compatible with Fe-type skarn deposits (Fig. 6). Ore in the Sivrikaya area is magnetite- and hematite-dominated with a limited amount of sulfide (pyrite and chalcopyrite) inclusions (Fig. 4e and f). This is quite compatible with the finding of Einaudi et al. (1981) that oxidized skarns are characteristically magnetite-dominated.

8.4. Source of hydrothermal solutions

The range of Te in first-stage inclusions is close to the eutectic temperature of H_2O–$CaCl_2$ systems (Shepherd et al., 1985), which indicates that $CaCl_2$ is included in the hydrothermal fluids dominantly (Roedder, 1984). Salinity and Th temperature of this stage of inclusion are higher than those of other stages. The presence of $CaCl_2$ has been considered by many researchers (Neng et al., 1999; Germann et al., 2003) as an indication of direct or indirect interaction with either seawater or marine sediments in the surrounding area. The limestone layer in the skarn contacts is the only reasonable source for the $CaCl_2$-containing first-stage inclusions. Through later stages, $CaCl_2$-dominated fluid inclusions were changed to a mixture of $MgCl_2$–H_2O (−33.6 °C), KCl–NaCl–H_2O (−23.5 °C) and NaCl–H_2O (−21.2 °C) water salt

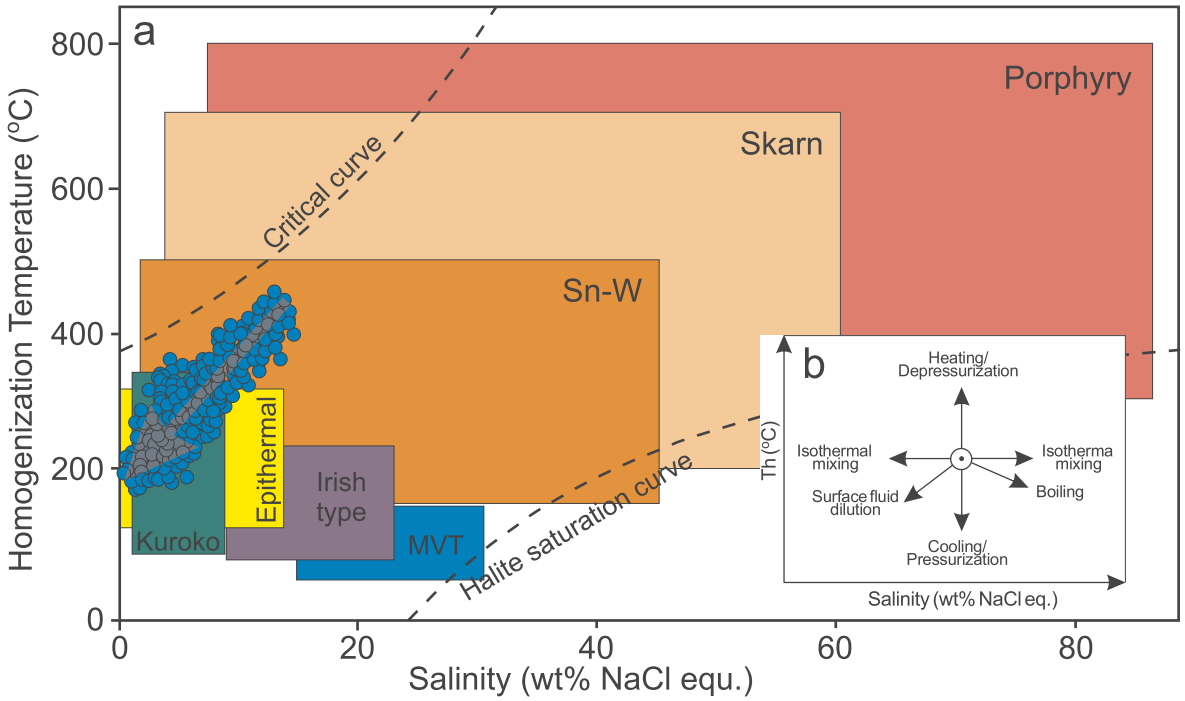

Fig. 14. a) Comparision of T_h and salinity (wt% NaCl equ.) values of fluid inclusions from Sivrikaya skarn mineralization with typical range of fluid inclusions from different deposit types; b) schematic diagram showing typical trends in T_h–salinity space due to various fluid evolution processes (Wilkinson, 2001).

systems rather than the specific eutectic temperature of single phases. Finally, third-stage inclusions were determined to be NaCl-dominated according to the very close eutectic temperatures of the NaCl–H_2O system (Shepherd et al., 1985). The change from $CaCl_2$- to NaCl-dominated composition of the fluid inclusions from the first to the last stage suggests that the interaction of hydrothermal solutions with carbonaceous host rocks was high at the beginning of the skarnization. During the later stages, decreasing interaction between hydrothermal solutions and carbonates may have caused changes leading to NaCl-dominated compositions.

Higher salinity (up to 14.3 wt%) and Th temperatures (up to 462 °C) were determined in first-stage inclusions, and lower salinity and Th temperatures were recorded in third-stage inclusions. Decreasing salinity content versus Th temperatures of fluid inclusions was identified in all investigated minerals. This decreasing salinity trend corresponds to the mixture of meteoric water with hydrothermal solutions (Fig. 14a and b) (Wilkinson, 2001). These data clearly indicate that salinity content of hydrothermal solutions was comparatively higher at the early stage of skarnization due to the interaction between the magmatic origin of solutions and carbonaceous limestones. During the later stages, mixtures of meteoric water decreased the salinity content of the solutions as well as Th temperatures.

Carbon isotope values of skarn calcites in the Sivrikaya area (between −4.2 and 0.7‰) are very close to the characteristic range of marine carbonates (between −3 and +3‰, Fig. 12). On the other hand, $\delta^{13}C$ ratios of dolomitic limestones are slightly depleted (up to −6.5‰) compared to marine carbonates. Carbon isotopic composition of marine sedimentary rocks, as reported in pioneering studies, ranges between −3‰ and +3‰, while heavily depleted isotopic values range between −18‰ and −38‰ (Ohmoto, 1986; Hoefs, 2009). These highly depleted isotopic values were reported from organic material (mollusk shells, chemogenic carbonate, carbonate skeletons of fossils, etc.) rich sedimentary rocks (Bowman, 1998; Allegre, 2008). Slightly depleted $\delta^{13}C$ values of dolomitic limestones, (up to −6.5‰) as compared to marine carbonates, can be explained by the higher organic material in carbonates (Horacek et al., 2009). Considerable amounts of organic material in the dolomitic limestone (Fig. 3e and f) may have played an important role in the depletion of isotopic values. Decarbonatization trends of organic matter between dolomitic limestones and skarn calcites in both locations support this possibility (Fig. 12).

The $\delta^{18}O$ values of dolomitic limestones were found to be highly depleted compared to those of marine limestones, and further depleted $\delta^{18}O$ values of skarn calcite were also recorded (Fig. 12). The decreasing $\delta^{18}O$ trend was determined on the diagram of $\delta^{13}C_{PDB}$ vs. $\delta^{18}O_{SMOW}$, while $\delta^{13}C$ increased (Fig. 12). This negative correlation indicates that C isotopes were enriched in skarn calcite, whereas the O isotope was highly depleted compared to the dolomitic limestones. Highly depleted O isotopes can be explained by an influx of meteoric water in the shallow depth of skarnization (Criss and Taylor, 1986; Jamtveit and Anderson, 1993), but enrichment in C isotopes is still debated.

It has been noted by Ottoway et al. (1994) and Liu and Liu (1997) that the enrichment of carbon isotopes suggests that if CO_2 mainly originated from sedimentary organic matter, it should show C-enrichment and O-depletion, since organic matter can act as a reducing agent in a thermo-chemical sulfate reduction process (Ottoway et al., 1994; Zhou et al., 2013). Therefore, the reason for negative correlation between carbon and oxygen isotopes may be the contribution of sedimentary organic matter. The variation of carbon and oxygen isotopes between marine carbonates and magmatic rocks also indicates that the skarn calcite might have been formed by the interaction of magmatic hydrothermal fluids and carbonates in variable proportions. Additionally, as indicated above, the mixture of meteoric water was also deduced from the decreasing salinity content of the fluid inclusions.

8.5. Source of methane in the fluid inclusions

Higher amounts of organic materials in the sedimentary limestone are compatible with the enrichment of C-isotopes. However, if decarbonatization of organic materials exists in the system, CO_2 should have been detected in the fluid inclusions, but none of the CO_2 phase could be observed during microthermometric investigations of the fluid inclusions. However, it is already known that hydrofracturing and/or brecciation in the near-surface environment causes separation of a CO_2

Table 5
Comparison of skarn properties of this study with mostly known skarn locations in the northeastern and western parts of Turkey.

	Host Rock and Age	Intrusion and Age	Type of Skarn	Temperature °C	Oxidation/ Reduction	Garnet Compon. (mole %)	Pyroxene Compon. (mole %)	Mineral Assemblage	References
Sivrikaya This Study	Late Cretaceous carbonate	Late Cretaceous–Eocene granitoid	Exoskarn	166–462	Oxidized	Andradite $Adr_{79-99}Grs_{0-18}Prs_{1-3}$	Diopside $Di_{69-77}Hd_{22-30}Joh_{0-1}$	Grt, Px, Ep, Tr, Act, Mag, Hem, Qtz, Cal, Py, Ccp,	This study
Arnastal-Camiboğazı Gümüşhane	Late Cretaceous carbonate	Eocene granitoid	Exoskarn	329–558	Highly oxidized	Andradite $And_{72-100}Grs_{0-28}$	Diopside $Di_{97-99}Hd_{1-3}Jo_0$ $Wo_{51}En_{48-49}Fs_1$	Grt, Px, Ep, Ves, Phl, Mag, Hem, Py, Po, Qtz, Cal,	Sipahi (2011)
Özdil Yomra–Trabzon	Jurassic–Early Cretaceous marble	Jurassic-Early Cretaceous granitoid	Exoskarn	400–600	Oxidized	Andradite $And_{73-99}Grs_{1-27}$	Diopside $Di_{55-64}Hd_{30-41}Jo_{3-7}$ $Wo_{51-52}En_{39-43}Fs_{5-9}$	Grt, Px, Ep, Tr, Act, Mag, Hem, Py, Qtz, Cal,	Aslan, 1991; Sadıklar (1993)
Çambaşı Kabadüz–Ordu	Late Cretaceous marble	Late Cretaceous monzonite	Exoskarn	–	Oxidized	Grossular-Andradite $And_{1-56}Grs_{43-92}$	Diopside	Act, Mag, Py, Po, Qtz, Cal,	Saraç (2003)
Kotana Dereli–Giresun	Pre–Early Jurassic Marble	Late Cretaceous–Eocene monzogranite	Endo–Exoskarn	380–460	Oxidized	Andradite$And_{47-99}Grs_{0-51}$	Diopside $Di_{80-87}Hd_{9-15}Jo_{1-5}$ $Wo_{51-52}En_{39-43}Fs_{5-9}$	Grt, Cpx, Ep, Tr, Act, Am, Scp, Mag, Hem, Py, Po, Sp, Ccp, Qtz, Cal,	Çiftçi (2011); Saraç (2003)
Dağbaşı Araklı–Trabzon	Early Cretaceous Limestone	Late Cretaceous Dağbaşı Granitoid	Exoskarn	162-466	Oxidized	Prograde Grossular $And_{0-9}Grs_{56-79}Prs_{21-38}$ Retrograde Andradite $And_{75-100}Grs_{0-23}Prs_{0-4}$	Prograde stage $Hed_{22-32}Diy_{67-77}Joh_{0-1}$ Retrograde stage $Hed_{22-63}Diy_{0-36}Joh_{32-77}$	Py, Po, Ccp, Sp, Gn, Qtz, Cal,	Demir (2015); Demir and Dişli (2016)
Susurluk	Recrystallized limestone–marble Mesozoic	Çataldağ granitoid Oligomiocene	Endo–Exoskarn	371– > 600	Oxidized	Grossular-Andradite $And_{3-74}Grs_{23-91}Prs_{0-12}$	Diopside-Hedenbergite $Di_{20-96}Hd_{3-79}Jo_{0-7}$	Grt, Px, Ves, Wo, Ccp, Bn, Qtz, Cal,	Orhan and Mutlu (2009); Orhan et al. (2011)
Ayazmant Ayvalık–Balıkesir	Metamorphic rocks with carbonate lenses. Early Triassic	Kozak Intrusion Late Oligocene	Endo–Exoskarn	300–576	Oxidized	Early stage Grossular (Grs_{75-79}) Andradite (Grs_{36-38}) Late stage Andradite (Adr_{84-89})	Early stage Diopside (Di_{94-97}) Late stage Diopside (Di_{65-75})	Grt, Px, Ep, Act, Scp, Am, Phl, Mag, Py, Po, Ccp, Bn, Sp, Gn, Qtz, Cal,	Oyman (2010)
Eğrikar Torul–Gümüşhane	Late Cretaceous carbonate	Late Cretaceous Eğrikar granitoid	Endo–Exoskarn	160–380	Oxidized	Grossular Andradite– Andradite	Hedenbergite	Grt, Px, Ep, Tr, Act, Mag, Hem, Py, Ccp, Au, Bn, Dg, Qtz, Cal,	Yilmaz (2016)

vapor phase due to the sudden decrease in overlaying pressure (Meinert, 1992; Bowman, 1998). The immiscibility evidence of fluid inclusions in early stage quartz clarifies the absence of CO_2 gases in the fluid inclusions of the Sivrikaya skarn mineralization.

Although no separate gas phases were observed in fluid inclusions, limited amounts of dissolved CH_2 and CH_4 were detected by Raman spectroscopic studies in the early-stage fluid inclusions of quartz, garnet and epidote minerals (Fig. 11). These gases are not widespread because only three of 22 measured samples were found to contain these phases. Some possible sources of methane in hydrothermal systems have already been mentioned (Welhan, 1988; Tsunogai et al., 1998; Whiticar, 1999; Horacek et al., 2009), including thermal degradation, bacterially produced methane, outgassing of juvenile methane and inorganic synthesis. Thermal degradation of organic material is accepted as the most likely source of CH_4 and CH_2 in the Sivrikaya area when taking into account skarn properties, such as shallow emplacement of intrusion, intensive fracturing and brecciation, oxidant-type skarnization, influx of meteoric water, temperature conditions over 100 °C and higher amounts of organic materials (Welhan, 1988; Berner and Faber, 1993).

8.6. Comparisons with other skarn deposits

Skarn-type ore deposits in the northeastern region of Turkey are distributed along the margins of the Late Cretaceous–Eocene granitic intrusion (Fig. 1). Skarn formations are observed along two levels throughout the contact of these granitoids. The first-level skarn formation is formed along the margins of a granitic intrusion and a Late Cretaceous volcano-sedimentary unit, which includes a carbonate level (Çambaşı, Eğrikar, Arnastal-Camiboğazı and Kartiba). Second-level skarn formations are formed along the same granitic intrusion and older (Early Cretaceous–Jura-aged) carbonate rocks (Table 5).

Characteristic relationships between skarn type and garnet and pyroxene chemistry have been established. Andradite-rich garnet has been accepted as the indication for Fe-type skarn, while diopside-rich pyroxene indicates Fe–Cu-type skarn deposits (Einaudi et al., 1981; Meinert et al., 2005; Ciobanu and Cook, 2004). Magnetite- and hematite-dominated skarns and epidote involvement have been accepted as characteristic features of oxidant-type skarns in some studies (Einaudi et al., 1981). Although all of the skarns in the region are defined as oxidized type, there are significant differences in garnet and pyroxene composition, host rock properties, skarn types and mineral paragenesis.

The majority of skarn-type deposits in the northeast of Turkey are rich in andradite and diopside, and the dominant ore minerals are magnetite and hematite, with minor amounts of pyrite and chalcopyrite (Table 5). Although Kotana skarn is similar to the other skarns due to the andradite and diopside content, it contains considerable amounts of sulfide in addition to magnetite and hematite. On the other hand, grossular and hedenbergite were reported only from Eğrikar and Dağbaşı deposits, and higher amounts of sulfide phases were accompanied by magnetite and hematite in these deposits. Exoskarn-type mineralization was reported from most of the deposits, whereas both endoskarn and exoskarn mineralization were reported from Kotana and Eğrikar deposits.

Formation temperatures reported from Arnastal–Camiboğazı and Özdil ore deposits are somewhat higher than in the other ore locations in the region. However, since the temperatures reported from these deposits are based on thermometric calculations, they are far from representative of all mineralization stages. According to fluid inclusion measurements made in quartz minerals, the temperature values reported from the Eğrikar deposit are in the range of 160–380 °C (Yilmaz, 2016), and salinity values are in the range of 3.4–7.6 wt% NaCl equ., while temperature values reported from quartz and calcite minerals from the Kotana deposit range from 380 to 460 °C (Çiftçi, 2011), and salinity values are lower than 15 wt% NaCl equ. Considering the limited number of mineral phases (quartz and calcite) that were used, the temperature values given in these studies are also far from representative of all mineralization stages.

In this study, temperature values reported from garnet, epidote, quartz and calcite are in the range of 166–462 °C. These values are very close to the temperature values (between 162 and 466 °C) (Table 5) reported from the Dağbaşı skarn deposit (Demir, 2015) (Table 5). In addition to these measured temperature values, fluid inclusion studies, which represent different skarn stages and mineral phases, appear to contribute to revealing changes in the amount of salinity and possible salt compositions contained in hydrothermal solutions.

Comparing the skarn-type deposit in the northeastern region of Turkey with the oxidized-type Susurluk deposit in western Turkey, it appears that the Susurluk deposit has higher temperature and salinity values (Orhan et al., 2010). In addition, while the skarn deposits in the northeastern region of Turkey are related to the granitic intrusion developed in the Late Cretace–Eocene interval skarn deposits in western Turkey (Susurluk and Ayazmant) are related to the younger (Oligo-Miocene) granitic intrusions. Based on the host rock lithology, the Susurluk deposit was associated with Mesozoic-aged limestones, whereas the Ayazmant deposit was developed in the recrystallized marble contact in the metamorphic series (Oyman, 2010). The Susurluk skarn deposit differs from eastern-region skarn deposits in its high wollastonite content. On the other hand, molybdenum was observed in the Ayazmant skarn deposit, and a relationship between skarn deposit and porphyry and epithermal systems was described. In contrast, there are no porphyry and epithermal systems defined in the vicinity of the skarn deposits in northeastern Turkey, and wollastonite has not been reported.

Comparing the T_h and salinity values of Sivrikaya skarn with the characteristic range of these types of deposits worldwide (Wilkinson, 2001), it is apparent that Sivrikaya Fe-skarn mineralizations occurred at relatively low temperature and salinity conditions (Fig. 14a). The low temperature and salinity values reported from other skarn deposits in the northeastern region of Turkey (Egrikar, Dağbaşı and Kotana) are consistent with Sivrikaya skarn. Shallow depth inherited from oxidized-type skarnization and a mixture of meteoric water may have been responsible for these lower T_h and salinity conditions. The decreasing salinity content of the fluid inclusions with T_h supports this possibility.

The distribution of the skarns in northeastern Turkey is considerably higher at the contact between granitic intrusion and Late Cretaceous carbonates than at the contact between the same granitoid and Jurassic–Early Cretaceous carbonates. This is a consequence of the fact that contact between granitic intrusion and Late Cretaceous carbonates is much longer than the contact between the same granitic intrusions and Jurassic–Early Cretaceous carbonates. Late Cretaceous units are arranged in the order Çatak, Kızılkaya, Çağlayan and Trebolu formations, from bottom to top. Since the carbonate level is formed in the Çatak formation within these units, the contact of the granites with the Çatak formation can be used as a guide level in the determination of skarns in the region.

9. Summary and conclusions

The Sivrikaya skarn mineralization has developed along the carbonate level within the Late Cretaceous volcano-sedimentary unit and ikizdere granitoid, which was intruded in the Late Cretaceous–Eocene interval. The andradite-rich garnet and diopside-rich pyroxene composition, the presence of magnetite- and hematite-dominated ore, and accompanying epidotes indicate an oxidized-type mineralization.

The İkizdere plutonic rocks, possessing alkaline and metaluminous features, are closely associated with volcanic arc-related granitoides, and this type of plutonic rock is always responsible for the formation of Fe-type skarn occurrences. Additionally, the high vanadium and lower Rb/Sr ratios of the İkizdere granitoid are appropriate for Fe-type skarn-producing granitoid.

According to the fluid inclusion studies, the salt composition of

early-stage fluids was characterized by a $CaCl_2$-dominated system. The composition becomes NaCl-dominated towards the final stage of formation. The $CaCl_2$ content of the early stage may result from the interaction between hydrothermal solutions and carbonate host rocks.

The coexistence of fluid-rich and vapor-rich fluid inclusions in the early-stage quartz and measured temperature values in the range of similar intervals indicate that there is a boiling in the initial stage of the skarnization. Brecciated host rock at the macroscopic scale and highly fractured microscopic textures are indications of hydrofracturing after boiling.

The organic content of the carbonates observed along the skarn zone is quite high. It is believed that CH_4 and CH_2, which are observed in the composition of some fluid inclusions, are caused by the thermal degradation of organic material during the decarbonation of these carbonates. After the boiling, all of the CO_2 produced by the decarbonization process may have been removed from the system, while a limited amount of the CH_4 and CH_2 may have been enclosed in the fluid inclusions because the solubility of the CH_4 is higher than that of the CO_2 in the hydrothermal environment.

According to the fluid inclusion measurements, T_h temperatures reach up to 462 °C in the early stage, while the lower limit of these temperatures is around 166 °C in the last stage. The salinity content of the fluid inclusions increases up to 14.3 wt% NaCl equ. in the early stages and decreases to as low as 0.53 wt% NaCl equ. in the last stage. The positive correlation between salinity content and T_h temperatures can be explained by the presence of meteoric water in the system.

The variation of carbon and oxygen isotopes between marine carbonates and magmatic rocks also indicates that the skarn calcite might have been formed by the interaction of magmatic hydrothermal fluids and carbonates in variable proportions. In addition to magmatic hydrothermal fluids, the presence of meteoric water may have played an important role in the skarn mineralization.

Acknowledgements

This study was financially supported by the Scientific Research Foundation Council of Recep Tayyip Erdogan University (Project #2012.109.01.2). Useful suggestions were provided by the editor Franco Pirajno and by two anonymous referees. We would like to thank Dr. Melanie Kaliwoda of Ludwig Maximilian University for providing microprobe analyses for this study and Mustafa Aksu, Kadir Bayraktar and Ali Dişli for their help during the field work and sample preparation.

References

Akçay, M., Arar, M., 1999. Geology, mineralogy and geochemistry of the Çayeli massive sulphide ore deposit, Rize, NE Turkey. In: In: stanley (Ed.), Mineral Deposits: Processes to Processing Balkema, Rotterdam, pp. 459–462.

Akçay, M., Çavga, H., 1997. Geology, mineralogy and genesis of the auriferous quartz veins in the Olucak (Gümüşhane) area. Selçuk University 20th Anniversary Geology Symposium, Konya, pp. 189–202 (in Turkish with English abstract).

Allegre, C.J., 2008. Isotope Geology. Cambridge University Press, New York, pp. 534.

Aslan, N., Akçay, M., 2011. Geologic, mineralogic and geochemical charactericitics of Au-Ag deposits in Mastra (Gümüşhane). 64th Geological Congress of Turkey Abstracts, pp. 181–183.

Aslan, Z., 1991. Özdil (Yomra-Trabzon) yöresinin petrografisi skarn oluşukları ve granat-piroksen ritmikleri. KTÜ Fen Bilimleri Enstitüsü, Master thesis, Trabzon, 72 s.

Atamas, N.A., Yaremko, A.M., Seeger, T., Leipertz, A., Bienko, A., Latajka, Z., Ratajczak, H., Barnes, A.J., 2004. A study of the Raman spectra of alkanes in the Fermi-resonance region. J. Mol. Struct. 708, 189–195.

Aydın, F., 2014. Geochronology, geochemistry, and petrogenesis of the Maçka subvolcanic intrusions: implications for Late Cretaceous magmatic and geodynamic evolution of the eastern part of the Sakarya Zone, northeastern Turkey. Int. Geol. Rev. 56, 1246–1275.

Berner, U., Faber, E., 1993. Light hydrocarbons in sediments of the Nankai accretionary prism (leg 131, site 808). Proc. ODP Sci. Results 131, 185–195.

Bodnar, R.J., 1993. Revised equation and table for determining the freezing point depression of H_2O-NaCl solutions. Geochim. Cosmochim. Acta 57, 683–684.

Bowman, J.R., 1998. Stable isotope systematics of skarns, mineralized intrusion related skarn system. D.R., Lentz (Ed.), Mineralogical Association of Canada, Short course series, 26, 99–114.

Boztuğ, D., Ercin, A.I., Kuruçelik, M.K., Göç, D., İskenderoğlu, A., 2006. Geochemical characteristics of the composite Kaçkar batholith generated in a Neo-Tethyan cpnvergence system, eastern Pontides, Turkey. J. Asian Earth Sci. 27, 286–302.

Boztuğ, D., Jonckheere, R., Wagner, G.A., Yeğingil, Z., 2004. Slow Senonian and fast Paleocene-Early Eocene uplift of the granitoides in the cetral eastern Pontides, Turkey: apatite fission-track results. Tectonophysics 382, 213–228.

Burke, E.A.J., 2001. Raman microspectrometry of fluid inclusions. Lithos 55, 139–158.

Burt, D.M., 1972. Mineralogy and Geochemistry of Ca-Fe-Si Skarn Deposits. PhD thesis, Harvard University, p. 256, (unpublished).

Ciobanu, C.L., Cook, N.J., 2004. Skarn texture and a case study: the Ocna de Fier-Dognecea orefield, Banat, Romania. Ore Geol. Rev. 24, 315–370.

Clechenko, C.C., Valley, J.W., 2003. Oscillatory zoning in garnet from the Willsboro wollastonite skarn, Adirondacks mts, Newyork: a record of shallow hydrothermal processes preserved in granülite facies terane. J. Metamorphic Geol. 21, 771–784.

Criss, R.E., Taylor, H.P., 1986. Meteoric-hydrothermal systems. Rev. Mineral. 16, 373–424.

Çakır, M., 1986. İkizdere (Rize)- İspir (Erzurum) arasındaki Fe, Cu-Mo cevherleşmelerine ait maden jeolojisi raporu. MTA Rapor No: 8049.

Çınar, S., Kahraman, İ., Yılmaz, B.S., Çakır, M., 1986. Rize-ispir arasının maden jeolojisi raporu. MTA Rapor No: 8048.

Çiftçi, E., 2011. Sphalerite associated with pyrrhotite-chalcopyrite ore occurring in the Kotana Fe-skarn deposit (Giresun, NE Turkey): exolutions or replacement. Turk. J. Earth Sci. 20, 307–320.

Çiftçi, E., Hagni, R.D., 2005. Mineralogy of Lahanos deposit a Kuroko-type volcanogenic massive sulfide deposits from Eastern Pontides (Giresun-NE Turkey). Geol. Bull. Turkey 48 (1), 58–64.

Demir, Y., 2015. Mineral Chemical investigation of the Dağbaşı skarn occurrences (Trabzon, NE Turkey) WMESS, 7–11 September, Prague/Chech Republic.

Demir, Y., Uysal, I., Sadıklar, M.B., Ceriani, A., Hanilç, N., Müller, D., 2015. Mineralogy, mineral chemistry, fluid inclusion, and stable isotope investigations of the Kabadüz ore veins, Ordu, NE-Turkey. Ore Geol. Rev. 66, 82–98.

Demir, Y., Uysal, I., Sadıklar, M.B., Sipahi, F., 2008. Mineralogy, mineral chemistry, and fluid inclusion investigation of köstere hydrothermal vein-type deposit (Gümüşhane, NE-Turkey). Neues Jahrbuch für Mineralogie 185 (2), 215–232.

Demir, Y., Uysal, İ., Sadıklar, M.B., 2013. Mineral chemical investigation on sulfide mineralization of the Istala Deposit, Gümüşhane, NE-Turkey. Ore Geol. Rev. 53, 306–317.

Demir, Y., Dişli, A., 2016. Mineral chemistry and stable isotope (O, H and C) constraints of the Dağbaşı skarn occurrances (Trabzon, NE Turkey) WMESS, 5–9 September, Prague/Chech Republic.

Dipple, G.M., Gerdes, M.L., 1998. Reaction-infiltration feedback and hydrodynamics at the skarn front. Mineral. Assoc. Can., Short Course Series 26, 71–97.

Dokuz, A., 2011. A slab detachment and delamination model for the generation of Carboniferous high-potassium I-type magmatism in the Eastern Pontides, NE Turkey: Köse composite pluton. Gondwana Res. 19, 926–944.

Dokuz, A., Külekçi, E., Aydınçakır, E., Kandemir, R., Alçiçek, M.C., Pecha, M., Sünnetçi, K., 2017. Cordierite-bearing stronly peraluminous cebre rhyolite from the eastern sakarya zone, NE Turkey: Contraints on the variscan orogeny. Lithos 278–281, 285–302.

Dokuz, A., Karslı, O., Chen, B., Uysal, I., 2010. Sources and petrogenesis of Jurassic granitoids in the Yusufeli area, Northeastern Turkey: implications for pre- and post-collisional lithospheric thinning of the Eastern Pontides. Tectonophysics 480, 259–279.

Dokuz, A., Uysal, İ., Dilek, Y., Karslı, O., Meisel, T., Kandemir, R., 2015. Geochemistry, Re-Os isotopes and highly siderophile element abundances in the Eastern Pontide peridotites (NE Turkey): multiple episodes of melt extraction-depletion, melt rock interaction and fertilization of Rheic Ocean mantle. Gondwana Res. 27, 612–628.

Einaudi, M.T., Meinert, L.D., Newberry, R.J., 1981. Skarn deposits. Econ. Geol. 75, 317–391.

Einaudi, M.T., Burt, D.M., 1982. A special issue devoted to skarn deposits, Introduction terminology, classification and composition of skarn deposits. Econ. Geol. 77 (4), 745–754.

Evcimen, Ö., 2011. İkizdere Plütonunun (KD-Türkiye) U-Pb jeokronolojisi, petrolojisi ve jeodinamik evrimi, Gümüşhane Üniversitesi FBE, Master thesis, 92s.

Friedman, I., Oneil, J.R., 1977. Compilation of stable isotope fractionation factors of geochemical interest, Data of Geochemistry, United states government printing Office, Washington, p. 117.

Germann, K., Lüders, V., Banks, D.A., Simon, K., Hoefs, J., 2003. Late Hercynian polymetallic vein type base metal mineralization in the Iberian pyrite belt: fluid inclusion and stable isotope geochemistry (S-O-H-C). Miner. Deposita 38, 953–967.

Gökce, A., 2001. Fluid inclusion, Oxygen and Hydrogen isotope studies of the Çakmakkaya and Damarköy (Murgul - Artvin) copper deposits and their significances on the genesis of these deposits. Geol. Bull. Turk. 44 (2), 23–37.

Gökçe, A., Spiro, B., 2000. Sulfur isotope characteristics of the volcanogenic Cu-Zn-Pb deposits in the eastern pontide region, NE Turkey. Int. Geol. Rev. 42 (6), 565–576.

Gökçe, A., Spiro, B., 2002. Fluid-related characteristics of the Çakmakkaya and Damarköy copper deposits, northeast Turkey. Int. Geol. Rev. 44, 744–754.

Güven, İ.H., Nalbantoğlu, A.K., Takaoğlu, S., 1998. 1/100.000 ölçekli açınsama nitelikli Türkiye Jeoloji Harita Serisi.

Güven, İ.H., 1993. 1/250.000 scaled geological and metallogenical map of the Eastern Black Sea Region. General Directorate of Mineral Research and Exploration (in Turkish).

Hasançebi, N., 1993. Dağbaşı (Araklı-Trabzon) granitoyidine bağlı cevherleşmelerin incelenmesi, KTU, Fen Bilimleri Enstitüsü, Master Thesis, Trabzon, p. 65.

Hoefs, J., 1987. Stable Isotope Geochemistry, (3rd ed.): New York, Springer-Verlag, p. 241.

Hoefs, J., 2009. Stable isotope geochemistry (6th Edit). Springer Verlag, p. 285.

Horacek, M., Koike, T., Richoz, S., 2009. Lower Triassic $\delta^{13}C$ isotope curve from shallow marine carbonates in Japan, Panthalassa realm: confirmation of the Tethys $\delta^{13}C$ curve. J. Asian Earth Sci. 36, 481–490.

Jamtveit, B., 1991. Oscillatory zonation patterns in hydrrothermal grosslular-andradite garnet: nonlinear dynamics in regions of immiscibility. Amerikan Mineralogist 76,

1319–1327.
Jamtveit, B., Anderson, T., 1993. Contact metamorphism of layered shale carbonate sequences in the Oslo rift: III The natüre of skarn-forming fluids. Econ. Geol. 88, 1830–1849.
Joesten, R.L., 1974. Local equilibrium and metasomatic growth of zoned calc-silicate nodules from a contact aureole, christmas Mountains, Big region, Texas. Am. J. Sci. 274, 876–901.
Joesten, R.L., 1991. Kinetics of coarsening and diffusion controlled mineral growth. In: Kerrick, D.M. (Ed.), Contact Metamorphism, Reviews in Mineralogy, 26, pp. 507–582.
Kandemir, R., 2004. Gümüşhane yakın yörelerindeki Erken- Orta Jura yaşlı Şenköy Formasyonu'nun çökel özellikleri ve birikim koşulları. KTÜ, Fen Bilimleri Enstitüsü, PhD thesis, Trabzon, 274s.
Kandemir, R., Yılmaz, C., 2009. Lithostratigraphy, facies, and deposition environment of the lower Jurassic Ammonitico Rosso type sediments (ARTS) in the Gümüşhane area, NE Turkey: implications for the opening of the northern branch of the Neo-Tethys Ocean. J. Asian Earth Sci. 34 (4), 586–598.
Karslı, O., Chen, B., Aydın, F., Şen, C., 2007. Geochemical and Sr-Nd-Pb isotopic compositions of the eocene dölek and sariçiçek plutons, Eastern Turkey: implications for magma interaction in the genesis of high-K calc-alkaline granitoids in a post-collision extensional setting. Lithos 98, 67–96.
Karslı, O., Uysal, İ., Ketenci, M., Dokuz, A., Aydın, F., Kandemir, R., Wijbrans, J., 2011. Adakite-like granitoid porphries in eastern pontides, NE Turkey: potencial parental melts and geodynamic implications. Lithos 127, 354–372.
Karslı, O., Aydin, F., Sadiklar, M.B., 2004. The morphology and chemistry of Kfeldspar megacrysts from _Ikizdere Pluton: evidence for acid and basic magma interactions in granitoid rocks, NE Turkey. Chemie der Erde-Geochemistry 64, 155–170.
Karslı, O., Dokuz, A., Uysal, I., Aydin, F., Bin, C., Kandemir, R., Wijbrans, R.J., 2010a. Relative contributions of crust and mantle to generation of Campanian high-K calc-alkaline I-type granitoids in a subdution setting, with special reference to the Harşit pluton, Eastern Turkey. Contrib. Miner. Petrol. 160, 467–487.
Karslı, O., Dokuz, A., Uysal, I., Aydin, F., Kandemir, R., Wijbrans, R.J., 2010b. Generation of the Early Cenozoic adakitic volcanism by partial melting of mafic lower crust, Eastern Turkey: implications for crustal thickening to delamination. Lithos 114, 109–120.
Kaygusuz, A., Chen, B., Aslan, Z., Siebel, W., Şen, C., 2009. U-Pb SHRIMP ages, geochemical and Sr-Nd isotopic compositions of the Late Cretaceous I-type Sarıosman Pluton, Eastern. Turk. J. Earth Sci. 18 (4), 549–581.
Kırmacı, Z., Akdağ, K., 2005. Origin of dolomite in the Late Cretaceous-Paleocene limestone turbudite, Eastren Pontides, Turkey. Sed. Geol. 181, 39–57.
Korkmaz, S., 1993. Tonya-Düzköy (GB-Trabzon) Stratigrafisi. Türkiye Jeoloji Bülteni 36, 151–158.
Kurt, Y., 2014. Giresun, Bulancak Kirazören bölgesi skarn tipi demir yataklarının jeolojik, ve jeokimyasal incelenmesi, İstanbul Üniversitesi, Fen Bilimleri Enstitüsü, master thesis, İstanbul, p. 111.
Kwak, T.A.P., 1987. W-Sn skarn deposits and related metamorphic skarns and granitoids; in developments in economic geology, 24, Elsevier publishing company, p. 445.
Kwak, T.P.A., White, A.J.R., 1982. Contrasting W-Mo-Cu and W-Sn-F skarn types and related granitoids. Min. Geol. 32, 339–351.
Lin, F., Bodnar, R.J., Becker, S.P., 2007. Correlation of methane Raman v1 band position with fluid density and interaction at the molecular level. J. Raman Spectrosc. 38, 1510–1515.
Liu, J.m., Liu, J.J., 1997. Basin fluid genetic model of sediment-hosted microdisseminated gold deposits in the gold-triangle area between Guizhou, Guangxi and Yunnan. Acta Mineral. Sin. 17, 448–456.
Meinert, L.D., 1983. Variability of skarn deposits-quides to exploration, S.J. Boardman (Ed.), Revolution in the earth sciences: Kendal-Hunt Publishing, pp. 301–316.
Meinert, L.D., 1992. Skarn and skarn deposits. Geosci. Can. 19, 145–162.
Meinert, L.D., Diple, G.M., Nicolescu, S, 2005. World skarn deposits, Society of Economic Geologist, Inc., Economic Geology 100th Anniversary Volume, pp. 299–336.
Moore, W.J., McKee, E.H., Akıncı, Ö.T., 1980. Chemistry and chronology of plutonic rocks in the Pontid mountains, northern Turkey. In: Jankovic, S., Sillitoe, R.H. (Eds.), Eur. Copper Deposits, Belgrade, pp. 209–216.
Nakano, T., 1998. Pyroxene geochemistry as an indicator for skarn metallogenesis in Japan. In: Lentz, D.R., (Ed.), Mineralized intrusion-related skarn systems. Mineral. Assoc. Can., Short Course Series, 26, pp. 147–167.
Nakano, T., Yoshino, T., Shimazaki, H., Shimizu, M., 1994. Pyroxene composition as an indicator in the classification of skarn deposits. Econ. Geol. 89, 1567–1580.
Neng, J., Jiuhua, X., Mianxin, S., 1999. Fluid inclusion characteristics of mesothermal gold deposits in the Xiaoginling district, Shaanxi and Henan provinces, peoples republic of China. Mineral. Deposita 34, 150–162.
Newberry, R.J., 1983. The formation of subcalcic garnet in scheelite-bearing skarns. Can. Mineral. 21, 529–544.
Newberry, R.J., 1987. Use of intrusive and calc-silicate compositional data to distinquish contrasting skarn types in the Darwin polymetallic skarn district, California, USA. Miner. Deposita 22, 207–215.
Newberry, R.J., 1991. Scheelite-bearing skarns in the Sierra Nevada region, Calfornia: contrast in zoning and mineral compositions and tests of infiltration metasomatism theory. In: Barto-Kyriakidis, A. (Ed.), Skarns- Their Genesis and Metallogeny. Theophrastus Publications, Atkens, Greece, pp. 343–384.
Ohmoto, H., 1986. Stable Isotope geochemistry of ore deposits, In stable isotope in high temperature geological proceses. Rev. Mineral. Soc. Am. 16, 491–560.
Okay, A.I., Şahintürk, Ö., 1997. Geology of the Eastern Pontides, In: A.G. Robinson, (ed.), Regional and Petroleum Geology of the Black Sea and Surrounding Region, AAPG Mem., 68, pp. 291–311.
Orhan, A., Mutlu, H., 2009. Susurluk (Balıkesir) skarn yatağının mineralojik ve petrografik özellikleri. J. Eng. Arch. Facul. Eskişehir, Osmangazi University. 12 (2), 65–90.
Orhan, A., Mutlu, H., Fallick, A.E., 2011. Fluid infiltration effects on stable isotope systematics of the Susurluk Skarn deposit, NW Turkey. J. Asian Earth Sci. 40, 550–568.
Orhan, A., Mutlu, H., Hanilçi, N., 2010. Susurluk (Balıkesir) oksidan tip W-skarnının mikrotermometrik özellikleri. MTA Dergisi 141, 55–71.
Ortoleva, P.J., 1994. Geochemical self organization. Oxford Monographs on geology and geophysics, 23, p. 411.
Ottoway, T.L., Wicks, F.J., Bryndzia, L.T., 1994. Formation of the Muzo hydrothermal deposit in Colombia. Nature 369, 552–554.
Oyman, T., 2010. Geochemistry, mineralogy and genesis of the Ayazmant FeCu skarn deposit in Ayvalık, (Balıkesir), Turkey. Ore Geol. Rev. 37, 175–2001.
Özgür, N., 1993. Volcanogenic massive sulphide deposits in the East Pontic Metallotect, Ne Turkey. Resour. Geol. Special Issue 17, 180–185.
Pelin, S., 1977. Geologic investigation of southeast part of Alucra (Giresun) area for petrolium potential. Publication of Karedeniz Technical University, No: 87.
Potter, R.W., Clynne, M.A., Brown, D.L., 1978. Freezing point depression of aqueous sodium chloride solutions. Econ. Geol. 73, 284–285.
Revan, M.K., 2010. Determination of the typical properties of volcanogenic massive sulphide deposits in the eastern Black Sea Region, Hacettepe University, PhD Thesis, p. 320.
Roedder, E., 1984. Fluid inclusions: reviews in Mineralogy. Mineral. Soc. Am. 12, 12–45.
Sadıklar, M.B., 1993. Granat-pyroxene-rhythmite bei Özdil-Trabzon, NE-Türkei. Chemie de Erde 53, 341–353.
Sağlam, E.S., Akçay, M., 2016. Chemical and mineralogical changes of waste and tailings from the Murgul Cu deposit (Artvin, NE Turkey): implications for occurrance of acid mine drainage. Environ. Sci. Pollut. Res. 23, 6584–6607.
Saraç, S., 2003. Doğu Karadeniz Fe-skarn yataklarının karşılaştırmalı mineralojik ve jeokimyasal özellikleri, KTÜ, Fen Bilimleri Enstitüsü, PhD thesis, Trabzon, 259 s.
Shelton, K.L., 1983. Composition and origin of ore forming fluids in a carbonate hosted porphyry copper and skarn deposit: a fluid inclusion and stable isotope study of mines Gaspe, Quebec. Econ. Geol. 78, 387–421.
Shepherd, T.J., Rankin, A.H., Alderton, D.H.M., 1985. A Practical Guide to Fluid Inclusion Studies. Blackie, Glasgow, pp. 239.
Sipahi, F., 2011. Formation of skarns at Gümüşhane (Northeastern Turkey. N.Jb). Miner. Abh. 188–2, 169–190.
Sofracıoğlu, D., Kandemir, R., 2013. The Upper Cretaceous calciclastic submarine fan deposits in the Eastern pontides, NE Turkey: facies architecture and controlling factors. Turk. J. Earth Sci. 22, 588–610.
Şengör, A.M.C., Yilmaz, Y., Ketin, I., 1980. Remnants of pre-late jurassic ocean in northern Turkey: fragments of Permian-Triassic Paleo-Tethys. Geol. Soc. Am. 91, 599–609.
Taylor, B.E., 1976. Origin and significance of C-O-H fluids in the formation of Ca-Fe-Si skarn, Osgood Mountains, Humboldt country, Nevada, PhD thesis, Stanford university, Stanford, California, p. 149.
Topuz, G., Alther, R., Schwarz, W.H., Dokuz, A., Meyer, H.P., 2007. Variscan amphibolite facies rocks from the Kurtoğlu metamorpic complex. Gümüşhane area, Eastern Pontides, Turkey. Int. J. Earth Sci. 96, 861–873.
Topuz, G., Altherr, R., Siebel, W., Schwarz, W.H., Zack, T., Hasözbek, A., Barth, M., Satır, M., Şen, C., 2010. Carboniferous high-potassium I-type granitoid magmatism in the Eastern Pontides: the Gümüşhane pluton (NE Turkey). Lithos 116 (1–2), 92–110.
Tsunogai, U., Ishibashi, J., Wakita, H., Gamo, T., 1998. Methane-rich plumes in the Suruga Trough (Japan) and their carbon isotopic characterization. Earth Planet. Sci. Lett. 160, 97–105.
Tüysüz, N., 2000. Geology, Lithogeochemistry and genesis of the Murgul Massive Sulfide Deposit, NE-Turkey. Chem. Erde 60, 231–250.
Tüysüz, N., Sadıklar, B., Er, M., Yılmaz, Z., 1995. An epithermal gold-siver deposit in the Pontide island arc, Mastra-Gümüşhane, Northeast Turkey. Econ. Geol. 90 (5), 1301–1309.
Van den Kerkhof, A.M., Hein, U.F., 2001. Fluid inclusion petrography. Lithos 55, 27–47.
Vörös, A., Kandemir, R., 2011. A new Early Jurassic brachiopod fauna from Eastern Pontides (Turkey), N.Jb. Geol. Paleont. Abh., 260/3, pp. 343–363.
Welhan, J.A., 1988. Origins of methane in hydrothermal systems. Chem. Geol. 71, 183–198.
Whiticar, M., 1999. Carbon and hydrogen isotope systematics of bacterial formation and oxidation of methane. Chem. Geol. 161, 291–314.
Whitney, D.L., Evans, B.V., 2010. Abbreviations for names of rock forming minerals. Am. Mineral. 95, 185–187.
Wilkinson, J.J., 2001. Fluid inclusions in hydrothermal ore deposits. Lithos 55, 229–272.
Yardley, B.W.D., Lioyd, G.E., 1995. Why metasomatic fronts are really metasomatic sides. Geology 23, 53–56.
Yaylalı-Abanuz, G., Tüysüz, N., Akaryalı, E., 2012. Soil geochemical prospection for gold deposit in the Arzular area (NE Turkey). J. Geochem. Explor. 112, 107–117.
Yılmaz, C., Carannante, G., Kandemir, R., 2008. The rift-related Late Cretaceous drowning of the Gümüşhane carbonate platform (NE Turkey). Ital. J. Geosci. 127 (1), 37–50.
Yılmaz, C., Kandemir, R., 2006. Sedimentary Records of The Extensional Tectonic Regime With Temporal Cessation: Gümüşhane Mesozoic Basin (NE Turkey). Geol. Carpath. 57 (1), 3–13.
Yılmaz, M., 2016. Petrographical and geochemical investigations of the Eğrikar (Torul-Gümüşhane) Fe-Cu Skarn deposit, Gümüşhane Üniversitesi, Fen Bilimleri Enstitüsü, Master Thesis, Gümüşhane, p. 99.
Zhou, J., Huang, Z., Yan, Z., 2013. The origin of the Maozu carbonates-hosted Pb-Zn deposit, southwest China: constrained by C-O-S-Pb isotopic compositions and Sm-Nd isotopic age. J. Asian Earth Sci. 73, 39–47.